Article

A Very Large Telescope imaging and spectroscopic survey of the Wolf-Rayet population in NGC 7793*

Bibby, Joanne and Crowther, P. A.

Bibby, Joanne and Crowther, P. A. (2010) A Very Large Telescope imaging and spectroscopic survey of the Wolf-Rayet population in NGC 7793. Monthly Notices of the Royal Astronomical Society, 405 (4). pp. 2737-2753. ISSN 00358711*

Monthly Notices
of the
ROYAL ASTRONOMICAL SOCIETY

Mon. Not. R. Astron. Soc. **405,** 2737–2753 (2010) doi:10.1111/j.1365-2966.2010.16659.x

A Very Large Telescope imaging and spectroscopic survey of the Wolf–Rayet population in NGC 7793⋆

J. L. Bibby† and P. A. Crowther

University of Sheffield, Department of Physics & Astronomy, Hicks Building, Hounsfield Rd, Sheffield, S3 7RH

Accepted 2010 March 9. Received 2010 March 9; in original form 2010 February 9

ABSTRACT

We present a Very Large Telescope/Focal Reducer and Low Dispersion Spectrograph #1 (VLT/FORS1) imaging and spectroscopic survey of the Wolf–Rayet (WR) population in the Sculptor group spiral galaxy NGC 7793. We identify 74 emission-line candidates from archival narrow-band imaging, from which 39 were observed with the Multi Object Spectroscopy mode of FORS1. 85 per cent of these sources displayed WR features. Additional slits were used to observe H II regions, enabling an estimate of the metallicity gradient of NGC 7793 using strong line calibrations, from which a central oxygen content of $\log(\mathrm{O/H}) + 12 = 8.6$ was obtained, falling to 8.25 at R_{25}. We have estimated WR populations using a calibration of line luminosities of Large Magellanic Cloud stars, revealing ∼27 WN and ∼25 WC stars from 29 sources spectroscopically observed. Photometric properties of the remaining candidates suggest an additional ∼27 WN and ∼8 WC stars. A comparison with the WR census of the LMC suggests that our imaging survey has identified ∼80 per cent of WN stars and ∼90 per cent for the WC subclass. Allowing for incompleteness, NGC 7793 hosts ∼105 WR stars for which $N(\mathrm{WC})/N(\mathrm{WN}) \sim 0.5$. From our spectroscopy of H II regions in NGC 7793, we revise the global Hα star formation rate of Kennicutt et al. upward by 50 per cent to 0.45 $\mathrm{M}_{\odot}\ \mathrm{yr}^{-1}$. This allows us to obtain $N(\mathrm{WR})/N(\mathrm{O}) \sim 0.018$, which is somewhat lower than that resulting from the WR census by Schild et al. of another Sculptor group spiral NGC 300, whose global physical properties are similar to NGC 7793. Finally, we also report the fortuitous detection of a bright ($m_{\mathrm{V}} = 20.8$ mag) background quasar Q2358-32 at $z \sim 2.02$ resulting from C IV λ1548-51 redshifted to the λ4684 passband.

Key words: stars: Wolf–Rayet – ISM: H II regions – galaxies: individual: NGC 7793 – galaxies: stellar content – galaxies: ISM.

1 INTRODUCTION

Classical Wolf–Rayet (WR) stars are helium burning stars descended from massive O stars. Their strong stellar winds produce a unique broad emission-line spectrum, making WR stars easily identifiable in both Local Group (Massey & Johnson 1998) and more distant star-forming galaxies (Conti & Vacca 1990). WR stars contribute significantly to the chemical evolution of the interstellar medium (ISM) via stellar winds and core-collapse supernova (Dray & Tout 2003). Indeed, WR stars are believed to be the progenitors of Type Ib/c supernova and some long gamma-ray bursts; however, a direct observational link is yet to be established (Woosley & Bloom 2006).

WR stars can be divided into subtypes that are nitrogen-rich (WN) or carbon-rich (WC). Metal-rich environments are observed to favour WC stars due to stronger, metal-driven winds during both the WR (Crowther et al. 2002) and the progenitor O star phases (Mokiem et al. 2007), while we expect to find a higher fraction of WN stars in metal-poor environments (Massey & Johnson 1998). We can investigate the distribution of WR subtypes with respect to metallicity by studying galaxies spanning a range of metallicities. Indeed, many spiral galaxies possess a super-solar nuclei and sub-solar outer regions (e.g. Pagel & Edmunds 1981; Magrini et al. 2007).

It is thought that WN and WC stars are the progenitors of Type Ib and Ic SNe, respectively. The advent of 8-m class telescopes has allowed searches for WR populations to move beyond the Local Group (Schild et al. 2003). The identification of a Type Ib/c supernova progenitor is the long-term aim of our survey. The survey

⋆Based on observations made with ESO telescopes at the Paranal observatory under program ID 081.B-0289 and archival NASA/ESA *Hubble Space Telescope* data sets, obtained from the ESO/ST-ECF Science Archive Facility.

†E-mail: j.bibby@sheffield.ac.uk

consists of 10 nearby star-forming galaxies, and one dwarf irregular galaxy, which were largely chosen based on criteria such as distance, star formation rate (SFR) and orientation. To date, five galaxies in our sample have been completed (Schild et al. 2003; Hadfield et al. 2005; Hadfield & Crowther 2007; Crowther & Bibby 2009 & this work), whilst three are underway and three are in the preliminary stages.

By surveying ∼10 galaxies within 10 Mpc, our overall aim is to produce a complete catalogue of $\geq 10^4$ WR stars which can be referred to when a Type Ib/c supernova occurs. O stars have lifetimes of 3–10 Myr, of which ∼0.5 Myr is spent in the WR phase (Crowther 2007). Given this short lifetime, statistically we would expect at least one of the stars in our sample to undergo core-collapse producing a Type Ib (H-poor) or Type Ic (H, He-poor) SNe within the next few decades. Kelly, Kirshner & Pahre (2008) investigate the location of different classes of supernovae relative to the light distribution of the host galaxy which supports different progenitors for Type Ib and Ic SNe. Leloudas et al. (2010) extend this investigation to the distribution of WR subtypes with respect to the light distribution of two galaxies (M83 and NGC 1313) in our sample. They find WC stars to favour the brighter regions, consistent with the prediction that WC stars are progenitors of Type Ic SNe. Moreover, early-type WN (WNE) stars are found to be more consistent with the distribution of Type Ib SNe and are ruled out as Type Ic SNe progenitors.

NGC 7793 is an SA(s)d galaxy (de Vaucouleurs et al. 1991) that is a part of the Sculptor group of galaxies at a distance of 3.91 Mpc (Karachentsev et al. 2003). Despite its relatively low SFR ($0.3\,M_{\odot}\,yr^{-1}$, Kennicutt et al. 2008), its low distance and favourable orientation make it an appropriate addition to our galaxy survey. Previous spectroscopic observations (using the Anglo-Australian 4m telescope) of 4 H II regions within NGC 7793 have detected weak, broad He II λ 4686 emission (Chun 1983). However, no comprehensive WR survey has been undertaken to date. Previous, albeit few, observations of H II regions within NGC 7793 suggest that it has a shallow metallicity gradient (Webster & Smith 1983).

In this paper, we use Very Large Telescope (VLT) optical imaging and spectroscopy, combined with archival VLT and *Hubble Space Telescope* (*HST*) images to determine the massive stellar content of NGC 7793. Details of observations of NGC 7793 are presented in Section 2, including details of WR candidate selection. In Section 3, we discuss the properties of the nebular, whilst stellar properties and WR subtypes are determined in Section 4. Section 5 provides a comparison between ground- and space-based observations and addresses the completeness of our survey in relation to WR stars in the Large Magellanic Cloud (LMC). A discussion of Giant H II regions follows in Section 6, whilst Section 7 reports the serendipitous detection of a background quasar Q2358-32. Section 8 discusses the global WR population of NGC 7793 and is compared with the WR content of NGC 300, another Sculptor group spiral and other nearby galaxies. The paper concludes with a brief summary in Section 9.

2 OBSERVATIONS AND DATA REDUCTION

Imaging and spectroscopy of NGC 7793 were obtained in 2008 July and September using the Focal Reducer and Low Dispersion Spectrograph #1 (FORS1) mounted at the European Southern Observatory (ESO) VLT. In addition, archival VLT/FORS1 images were used and supplemented with *Hubble Space Telescope* (*HST*) Advanced Camera for Surveys (ACS) optical images.

2.1 VLT/FORS1 imaging

Broad-band *B*- and *V*-high throughput images plus narrow-band Hα and continuum images were obtained in 2008 July (270 s exposure) under good conditions (FWHM = 0.75 arcsec) using the two E2V blue-sensitive chips on FORS1 with a 6.8×6.8 arcmin^2 field of view and a pixel scale of 0.25 arcsec pixel^{-1}. A log of the observations is shown in Table 1. These images were reduced using standard procedures (bias subtraction and flat fielding) within Image Reduction and Analysis Facility (IRAF; Tody 1986).

In addition, archival narrow-band He II $\lambda_c = 4684$ Å imaging of NGC 7793 was available via the ESO archive along with [O III] continuum ($\lambda_c = 5100$ Å) images, offset from the [O III] λ5007 line by 6000 km s^{-1}. These were taken with VLT/FORS1 (program ID 70.D–0137(A)) under average seeing conditions (1.1–1.3 arcsec^2). The 6.8×6.8 arcmin^2 (0.2 arcsec pixel^{-1}) field of view was covered by one 2 k × 2 k Tektronix CCD. Due to the different detectors used on FORS1 the archival images have a different field of view to our own images, as shown in Fig. 1.

2.2 *H*ST/ACS imaging

Ground-based data were supplemented with high-resolution archival *HST*/ACS imaging taken from program 9774 (PI: Larsen,

Table 1. VLT/FORS1 observational log for NGC 7793. The seeing is calculated from the full width at half-maximum (FWHM) of bright, unsaturated, stars in the field of view.

Date	Filter/ mask ID	λ_c (Å)	Proposal ID/ PI	Exposure time (s)	Seeing (arcsec)
		Imaging			
2002-11-01	He II	4684	70.D-0137(A)	800	1.3
	[O III]/6000	5100	/ Royer	800	1.1
2008-07-05	H α	6563	081.B-0289(D)	270	0.75
	H α/4500	6665	/ Crowther	270	0.75
	B high	4440		270	0.75
	V high	5570		270	0.75
		MOS Spectroscopy			
2008-07-09	MASK 1	5850	081.B-0289(E)	1650	1.25
	MASK 2	5850	/ Crowther	1650	1.25
2008-09-23	MASK 3	5850		1650	1.25

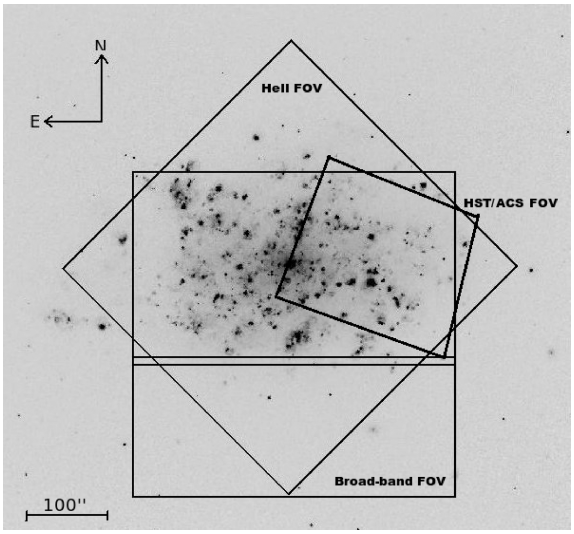

Figure 1. CTIO wide-field Hα image of NGC 7793 (Kennicutt et al. 2008), showing the field of view (FOV) of the B,V, Hα images ('broad-band'), archival He II & [O III] images, and the *HST*/ACS F555W images.

Mora et al. 2009). These images were obtained with the wide field channel (WFC) using the F555W filter with an exposure time of 680 s. The much improved spatial resolution allows us to accurately locate the source of the He II emission identified from FORS1 imaging in some instances (see Section 5.2). Other regions of NGC 7793 are covered by numerous *HST* pointings; however, *V*-band images are only available using the F555W filter of the region highlighted in Fig. 1.

2.3 FORS1 photometry & zero-points

Aperture photometry was performed using the DAOPHOT routine within IRAF. The photometric errors for objects within the narrow-band image range from ± 0.03 mag for bright ($m_{4684} = 20$ mag) sources to ± 0.34 mag for the faintest ($m_{4684} = 25$ mag) sources. For the broad-band images typical photometric errors range from ± 0.04 to 0.25 mag for bright ($m_v = 20$ mag) and faint ($m_v = 25$ mag) sources, respectively. Zero-points for the broad-band images were determined by comparing aperture photometry, obtained using the STARLINK package GAIA (Draper et al. 2009), of standard stars within the TPhe and PG1323-086 fields (Stetson 2000). The zero-point for the narrow-band Hα image was obtained in a similar way using the spectrophotometric standard star LTT 377 (Hamuy et al. 1992, 1994). The systematic error on the zero-point is ± 0.15 mag.

The calibration of the archival λ 4684 and λ 5100 images proved more challenging as standard stars were not obtained together with the NGC 7793 images. Given the central wavelength of the λ 5100 filter, we assumed that the λ 5100 mag corresponds to the average of the *B* and *V* magnitudes from which a zero-point was obtained. To calculate the zero-point for the λ 4684 images, we adopted $m_{4684} - m_{5100} = 0$ mag on average. The formal error on the overall zero-point applied to the λ 5100 and λ 4684 images was ± 0.18 mag.

With the exposure times shown in Table 1, the archival VLT/FORS1 He II λ 4684 imaging is complete to $m_{4684} = 22.85$ mag corresponding to $M_{4684} = -5.76 \pm 0.18$ mag for a distance of 3.91 Mpc (Karachentsev et al. 2003) and an average extinction of $E(B-V) = 0.179 \pm 0.024$ mag (see Section 3.1). Similar values were obtained for the $\lambda_c = 5100$ continuum images.

2.4 Source selection

From our archival narrow-band imaging we identified 74 emission-line sources using the 'blinking' method pioneered by Moffat & Shara (1983) and Massey & Conti (1983). DAOPHOT photometry revealed that ~25 per cent of our sources had multiple components. All sources and sub-regions are listed in Table 2 together with the corresponding photometry, we label the brightest components 'a', followed by 'b' etc. In 63 of the WR candidate regions, at least one of the multiple components showed an excess at λ 4684 (He II/C III emission) with respect to the λ 5100 continuum emission up to 2.43 mag. An additional 10 regions could only be detected in the λ_c 4684 filter. DAOPHOT could not achieve photometry of one candidate (#14) identified from the 'blinking' method due to the spatially extended nature of the λ_c 4684 emission.

Higher spatial resolution broad-band VLT imaging, obtained at the same time as the spectroscopy, enabled $B-V$ colours to be determined. A colour-cut of $E(B-V) \leq 0.4$ mag was applied for all sources that lay within the field of view of the broad-band image (recall Fig. 1) to exclude very red sources. The spatial location of the WR candidates in NGC 7793 is shown in Fig. 2, with the corresponding finding chart ID listed in Table 2. More detailed finding charts are available electronically (see supporting information). The deprojected distance from the centre of the galaxy, r/R_{25}, was calculated using an inclination of $i = 53.7^\circ$ and position angle of the major axis PA $= 99.3^\circ$ (Carignan & Puche 1990), with $R_{25} = 4.65$ arcmin (de Vaucouleurs et al. 1991; Corwin, Buta & de Vaucouleurs 1994).

2.5 Spectroscopy, flux calibration & slit losses

VLT/FORS1 Multi Object Spectroscopy (MOS) was undertaken in 2008 July with the standard resolution collimator and the 300 V grism (dispersion of ~3 Å pixel^{-1}) at a central wavelength of λ 5850. Spectra were obtained using 0.8 arcsec slits resulting in a spectral resolution of ~8 Å, with seeing conditions between 1 and 1.25 arcsec. The typical wavelength range of each slit was 3600–9200 Å; however, fringing effects made data longward of 7000 Å unreliable.

Each of the MOS masks that were designed contained 19 slits with lengths ranging from 22 to 26 arcsec and used exposure times of 1650 s. Due to the spatial distribution of our candidates only ~13 slits per mask could be placed on our primary sources. The remaining slits were used to obtain either multiple spectra of a candidate or a H II region. Out of the 74 candidates, we obtained spectra of 39 of our WR candidates in Table 2, some containing multiple sub-regions.

Spectroscopic data were bias subtracted and extracted using IRAF, whilst wavelength and flux calibration were achieved with FIGARO. Wavelength calibration was achieved from an He HgCdAr arc lamp. Spectrophotometric standard stars LTT 377 (masks nos 1 & 2) and LTT 1788 (mask no. 3) (Hamuy et al. 1994, 1992) were used to produce a relative flux calibration, whilst an absolute flux calibration was determined from comparison between the synthetic magnitudes and photometry. The synthetic magnitudes were obtained from the convolution of spectra with appropriate filters. This factor corrects our spectroscopic magnitudes for slit losses, which we determine to be 1.49 ± 0.3.

Table 2. Catalogue of WR candidates in NGC 7793 ordered by right ascension. Absolute magnitudes are derived using a distance of 3.91 Mpc (Karachentsev et al. 2003). Where spectra have been obtained, the derived $E(B-V)$ is used. For those sources with no nebular lines seen an average $E(B-V) = 0.18$ mag is used. For cases without spectroscopic observation, we provide photometric classifications (in parentheses). Association with H II regions relates to the catalogue of Davoust & de Vaucouleurs (1980).

ID	RA J2000	Dec. J2000	r/R_{25}	m_V mag ±	$m_B - m_V$ mag ±	m_{4684} mag ±	m_{4684}–m_{5100} mag ±	$E(B-V)$ mag	M_V mag	M_{4684} mag	Spectral Type	H II region	Finding Chart
1	23:57:31.543	−32:35:00.29	0.88	n/a	n/a	20.28 0.02	−0.11 0.07	0.18	n/a	−8.33	H II region	D1	1
2	23:57:33.067	−32:35:45.77	0.76	20.96 0.07	−0.15 0.08	20.69 0.03	−0.13 0.07	0.18	−7.56	−7.92	(not WR?)	–	1
3	23:57:35.837	−32:33:43.87	0.95	20.40 0.09	−0.01 0.09	20.12 0.05	−0.28 0.06	0.18	−8.12	−8.49	H II region	D2	1
4	23:57:37.240	−32:35:00.03	0.62	22.48 0.07	−0.12 0.08	21.19 0.02	−1.40 0.08	0.13	−5.88	−7.24	WC4–6	–	1
5b	23:57:38.858	−32:36:11.06	0.53	20.41 0.07	−0.25 0.12	20.15 0.03	−0.01 0.07	0.18	−8.11	−8.45	(not WR?)	D8	6
5a	23:57:38.942	−32:36:11.27	0.53	19.53 0.08	0.14 0.10	19.45 0.03	−0.02 0.04	0.18	−8.99	−9.16	(not WR?)	D8	6
6	23:57:39.049	−32:36:50.94	0.65	20.11 0.06	0.43 0.10	20.23 0.03	−0.06 0.07	0.18	−8.41	−8.38	H II region	–	6
7a	23:57:39.381	−32:35:58.98	0.49	20.25 0.06	−0.28 0.11	20.00 0.03	−0.15 0.07	0.18	−8.27	−8.61	H II region	D10	6
7b	23:57:39.450	−32:35:59.03	0.48	20.81 0.06	−0.16 0.17	21.01 0.06	−0.23 0.18	0.18	−7.71	−7.60	H II region	D10	6
8	23:57:39.532	−32:37:24.42	0.79	20.97 0.01	−0.21 0.21	20.72 0.01	−0.43 0.03	0.18	−7.55	−7.89	WN10	–	11
9	23:57:40.257	−32:36:35.08	0.55	21.12 0.01	−0.22 0.03	20.29 0.01	−0.79 0.14	0.00	−6.84	−7.67	WN8	D11	6
10	23:57:40.827	−32:35:36.48	0.40	20.17 0.07	0.03 0.13	19.29 0.05	−0.65 0.30	0.13[3]	−8.18	−9.14	WN2–4b	D12	6
11c	23:57:41.105	−32:34:50.26	0.47	20.73 0.07	0.06 0.11	20.21 0.05	−0.35 0.09	0.00		−7.75	H II region	D14	3
11b	23:57:41.197	−32:34:50.34	0.47	20.12 0.10	−0.06 0.13	20.15 0.08	−0.24 0.09	0.00	−7.84	−7.81	(WN?)	D14	3
11a	23:57:41.250	−32:34:51.19	0.46	19.20 0.08	0.07 0.13	19.38 0.04	−0.22 0.06	0.00	−8.76	−8.58	H II region	D14	3
12b	23:57:41.158	−32:35:50.17	0.40	20.17 0.06	0.11 0.11	20.01[1] 0.04[1]		0.18	−8.35	−8.60[1]	(not WR?)	D13	6
12a	23:57:41.165	−32:35:51.11	0.40	19.57 0.09	−0.09 0.12	19.08 0.05	−0.31 0.11	0.18	−8.95	−9.53	(WN?)	D13	6
13	23:57:41.340	−32:35:52.79	0.39	19.32 0.05	0.11 0.17	19.20 0.03	−0.10 0.03	0.18	−9.20	−9.41	(Not WR?)	D13	6
14	23:57:41.417	−32:35:35.97	0.37	21.27 0.07	0.05 0.07	–	–	0.30	−7.61		WC4	D15	6
15	23:57:41.738	−32:37:17.16	0.71	22.28 0.02	−0.06 0.18	21.49 0.02	−0.76 0.03	0.18	−6.24	−7.12	(WN?)	D17	11
16	23:57:42.040	−32:37:15.88	0.70	21.35 0.06	−0.21 0.08	20.55 0.04	−0.64 0.04	0.26	−7.43	−8.36	WN2–4	D17	11
17	23:57:43.254	−32:35:49.49	0.31	19.84 0.08	−0.07 0.10	19.63 0.04	−0.24 0.04	0.18	−8.68	−8.98	(WN?)	D20	6
18	23:57:43.434	−32:33:38.17	0.74	22.05 0.07	−0.01 0.07	21.54 0.04	−0.37 0.09	0.18	−6.47	−7.07	(WN?)	–	2
19b	23:57:44.072	−32:36:31.77	0.44	20.38 0.06	−0.27 0.08	19.68 0.04	−0.43 0.14	0.18	−8.14	−8.93	(WN?)	D23	11
19a	23:57:44.092	−32:36:32.53	0.44	19.82 0.03	−0.01 0.07	19.36 0.04	−0.66 0.05	0.18	−8.70	−9.25	(WN?)	D23	11
20	23:57:44.329	−32:35:53.13	0.27	22.50 0.05	−0.04 0.18	20.98 0.02	−1.51 0.03	0.18	−6.02	−7.63	WC4	D25	9
21a	23:57:44.416	−32:35:17.09	0.25	19.64 0.11	0.35 0.15	19.70 0.04	−0.17 0.23	0.18	−7.85	−8.59	(not WR?)	–	5
21b	23:57:44.416	−32:35:19.87	0.24	20.89 0.04	−0.10 0.01	20.02 0.07	−0.17 0.18	0.18	−7.63	−8.11	(not WR?)	–	5
22b	23:57:44.413	−32:35:52.01	0.27	21.51[2] 0.07[2]		21.16[1] 0.07[1]		0.18	−7.19[2]	−7.44[1]	H II region	D25	9
22a	23:57:44.491	−32:35:51.87	0.26	20.10 0.06	−0.11 0.11	19.85 0.04	−0.32 0.10	0.18	−8.42	−8.76	H II region	D25	9
22c	23:57:44.588	−32:35:51.56	0.26	21.43[2] 0.10[2]		21.26[1] 0.05[1]		0.18	−7.27[2]	−7.35[1]	(WN?)	D25	9
23	23:57:45.610	−32:36:56.14	0.55	23.15 0.03	−0.19 0.06	21.07 0.02	−2.43 0.05	0.14	−5.21	−7.35	WC4	–	11
24	23:57:46.647	−32:36:00.28	0.24	21.90 0.02	0.11 0.03	21.18 0.02	−0.77 0.05	0.18	−6.62	−7.43	WC4	D36	5
25	23:57:46.805	−32:34:06.49	0.50	21.81 0.04	−0.06 0.05	20.44 0.03	−1.09 0.05	0.18	−6.71	−8.17	WC4	–	2
26	23:57:47.049	−32:35:48.11	0.17	22.49 0.06	−0.16 0.09	21.44 0.03	−1.01 0.10	0.17[3]	−5.99	−7.12	WC4–6	–	5
27	23:57:47.868	−32:34:06.32	0.49	22.42 0.08	−0.11 0.12	21.49 0.04	−0.55 0.07	0.18[3]	−6.10	−7.12	WC4	D51	2

Table 2 – *continued*

ID	RA J2000	Dec. J2000	r/R_{25}	m_V mag ±	m_B-m_V mag ±	m_{4684} mag ±	$m_{4684}-m_{5100}$ mag ±	$E(B-V)$ mag	M_V mag	M_{4684} mag	Spectral Type	H II region	Finding Chart
28	23:57:47.933	−32:33:41.44	0.63	21.22 0.07	−0.10 0.54	20.74 0.03	−0.28 0.07	0.18	−7.31	−7.87	(WN?)	D50	2
29b	23:57:48.064	−32:34:29.28	0.35	19.53 0.05	−0.14 0.30	19.12 0.03	−0.08 0.19	0.18	−8.99	−9.42	(not WR?)	D52	4
29a	23:57:48.184	−32:34:29.49	0.34	19.08 0.01	0.08 0.03	18.85 0.02	−0.04 0.06	0.18	−9.44	−9.76	(not WR?)	D52	4
29c	23:57:47.943	−32:34:29.45	0.35	20.43 0.07	0.09 0.13	19.90 0.05	−0.16 0.09	0.18	−8.09	−8.71	(not WR?)	D52	4
29d	23:57:48.035	−32:34:31.40	0.33	20.63 0.10	0.05 0.11	20.19 0.05	−0.69 0.32	0.18	−7.89	−8.71	(WN?)	D52	4
30b	23:57:48.376	−32:34:33.60	0.32	21.01 0.09	−0.10 0.14	20.55 0.05	−0.55 0.09	0.18	−7.51	−8.06	(WN?)	D55	4
30a	23:57:48.479	−32:34:33.48	0.32	20.40 0.08	−0.18 0.14	19.98 0.03	−0.23 0.07	0.18	−8.12	−8.63	(WN?)	D55	4
31b	23:57:48.487	−32:37:01.57	0.58	20.31 0.06	−0.41 0.16	19.51 0.05	−0.42 0.15	0.18	−8.21	−9.10	(WN?)	D53	14
31a	23:57:48.535	−32:37:02.62	0.59	19.75 0.05	−0.31 0.15	19.33 0.04	−0.22 0.05	0.18	−8.77	−9.28	(WN?)	D53	14
31c	23:57:48.665	−32:37:02.84	0.59	20.48 0.09	−0.08 0.14	19.95 0.07	−0.45 0.07	0.18	−8.04	−8.66	(WN?)	D53	14
32b	23:57:48.560	−32:34:46.00	0.24	–	–	21.13 0.05	−1.19 0.08	0.18		−7.48	(WC?)	D54	8
32a	23:57:48.644	−32:34:46.86	0.23	20.94 0.10	0.00 0.12	20.84 0.03	+0.13 0.06	0.18	−7.57	−7.77	(not WR?)	D54	8
33	23:57:48.791	−32:34:35.37	0.30	19.56 0.04	−0.16 0.07	19.15 0.02	−0.25 0.09	0.18	−8.96	−9.21	(WN?)	D55	4
34	23:57:48.816	−32:34:53.27	0.19	18.07 0.01	−0.21 0.01	17.72 0.01	−0.18 0.24	0.32[3]	−10.88	−11.39	WN5–6:WC4	GHR #3	8
35	23:57:48.855	−32:34:32.86	0.31	21.57 0.09	0.01 0.46	20.61 0.04	−0.59 0.16	0.09[3]	−6.66	−7.66	WC5–6	D55	4
36	23:57:48.891	−32:34:57.03	0.17	20.88 0.02	0.06 0.05	20.20 0.04	−0.90 0.06	0.27	< −4.98	−8.74	WC6	–	8
37	23:57:48.958	−32:36:58.16	0.56	21.22 0.08	0.00 0.12	20.43 0.08	−0.74 0.10	0.13	−7.16	−8.00	WC4–6	D53	14
38	23:57:49.051	−32:33:32.36	0.67	22.90 0.05	–0.07 0.06	21.86 0.03	−0.84 0.06	0.18	−5.62	−6.75	(WN?)	–	2
39	23:57:51.522	−32:35:01.33	0.15	–	–	20.77 0.04	−0.44 0.06	0.18[3]		−7.84	WN2–4	D75	10
40	23:57:52.025	−32:35:21.30	0.12	19.70 0.04	−0.05 0.39	18.98 0.05	−0.56 0.23	0.18	−8.81	−9.63	(WN?)	D82	10
41	23:57:53.045	−32:35:13.44	0.17	21.43 0.05	−0.12 0.09	20.71 0.03	−0.48 0.10	0.18	−7.09	−7.90	(WN?)	D85	10
42b	23:57:53.540	−32:36:42.24	0.54	20.99 0.09	0.22 0.10	20.40 0.04	−0.57 0.07	0.29	−7.86	−8.60	⊐WC4	D88	16
42a	23:57:53.621	−32:36:42.98	0.54	20.65 0.07	−0.03 0.13	20.34 0.03	−0.12 0.17	0.29	−8.20	−8.66		D88	16
43	23:57:53.975	−32:35:15.25	0.21	23.29 0.09	0.16 0.12	21.61 0.03	−1.39 0.12	0.18		−7.00	WC4–6	–	10
44	23:57:54.090	−32:35:46.91	0.28	–	–	22.39 0.11	−1.64 0.14	0.18		−6.22	(WC?)	D91	10
45	23:57:54.122	−32:35:27.83	0.22	–	–	22.11 0.06	–	0.18		−6.50	WC4–6	–	10
46	23:57:54.325	−32:34:00.33	0.51	20.10 0.07	−0.02 0.08	19.48 0.02	−0.78 0.06	0.17	−8.38	−9.09	WC4	D95	7
47	23:57:54.704	−32:35:30.35	0.25	21.04 0.03	−0.32 0.12	19.92 0.03	−0.73 0.06	0.17[3]	−7.44	−8.65	WC6	D97	10
48	23:57:54.849	−32:35:29.64	0.26	20.02 0.02	−0.05 0.12	19.56 0.05	−0.34 0.08	0.18	−8.50	−9.05	(WN?)	D97	10
49	23:57:55.219	−32:33:55.78	0.55	22.12 0.09	0.30 0.10	21.31 0.02	−1.01 0.09	0.18	−6.40	−7.30	WN3	D101	7
50c	23:57:55.838	−32:34:41.75	0.36	–	–	21.22 0.04	–	0.25[3]		−6.41	(WC?)	D106	13
50a	23:57:55.880	−32:34:41.25	0.36	20.90 0.04	−0.04 0.11	20.76 0.03	+0.10 0.05	0.25[3]	−7.84	−7.16	WC4	D106	13
50b	23:57:55.979	−32:34:43.09	0.36	21.22 0.06	−0.17 0.07	20.88 0.03	−0.06 0.05	0.25[3]	−7.52	−7.98	(not WR?)	D106	13
51	23:57:56.310	−32:36:12.84	0.47	22.90 0.07	0.08 0.12	20.89 0.05	−1.19 0.23	0.18	−5.62	−7.72	(WC?)	D109	15
52a	23:57:56.875	−32:33:47.67	0.62	20.04 0.06	−0.04 0.08	19.75 0.03	−0.20 0.07	0.18	−8.48	−8.86	(WN?)	D111	7
52b	23:57:56.919	−32:33:46.60	0.63	20.19 0.05	0.04 0.08	20.05 0.03	−0.09 0.22	0.18	−8.33	−8.56	(not WR?)	D111	7
53	23:57:57.171	−32:36:08.72	0.49	19.70 0.05	–0.19 0.08	19.60 0.02	−0.10 0.35	0.18	−8.82	−9.01	(not WR?)	D110	15
54	23:57:57.205	−32:36:11.12	0.50	20.56 0.06	0.09 0.12	20.21 0.03	−0.40 0.03	0.18	−7.96	−8.40	(WN?)	D110	15
55	23:57:57.649	−32:35:39.16	0.41	23.84 0.08	−0.40 0.12	21.52 0.02	–	0.18	−4.68	−7.09	WC5–6	–	15
56	23:57:57.867	−32:34:50.81	0.41	23.46 0.06	−0.29 0.10	21.79 0.03	–	0.18	−5.06	−6.82	WN2–4	–	13

Table 2 – *continued*

ID	RA J2000	Dec. J2000	r/R_{25}	m_V mag ±	m_B-m_V mag ±	m_{4684} mag ±	$m_{4684}-m_{5100}$ mag ±	$E(B-V)$ mag	M_V mag	M_{4684} mag	Spectral Type	H II region	Finding Chart
57	23:57:58.175	−32:35:40.98	0.44	21.96 0.10	0.12 0.10	20.78 0.03	–	0.18	−6.56	−7.83	(WC?)	–	15
58a	23:57:58.548	−32:34:32.92	0.48	20.12 0.07	–0.04 0.14	19.71 0.04	−0.12 0.51	0.18	−8.40	−8.90	(not WR?)	D115	13
58b	23:57:58.602	−32:34:30.72	0.49	20.41 0.07	–0.05 0.11	20.14 0.04	+0.01 0.09	0.18	−8.11	−8.47	(not WR?)	D115	13
59	23:57:58.635	−32:35:46.19	0.47	23.21 0.06	–0.35 0.08	21.50 0.03	–	0.00	−4.75	−6.46	WC6	D116	15
60	23:57:58.929	−32:36:46.90	0.72	–	–	19.02 0.03	–1.35 0.13	0.18		−9.59	(WC?)	D117	18
61a	23:57:59.098	−32:36:50.32	0.74	19.72 0.04	−0.06 0.06	19.52 0.02	–0.09 0.06	0.18	−8.80	−9.09	(not WR?)	D118	18
61b	23:57:59.098	−32:36:48.96	0.74	19.96 0.05	0.00 0.07	19.74 0.03	–0.01 0.04	0.18	−8.56	−8.87	(not WR?)	D118	18
62	23:57:59.560	−32:36:42.42	0.72	22.16 0.05	0.28 0.06	21.41 0.02	−1.11 0.07	0.07	−6.02	−6.81	WN2–4	–	18
63	23:57:59.822	−32:34:23.47	0.55	23.38[2] 0.19[2]		22.04 0.04	−0.50 0.10	0.18	−5.32[2]	−6.57	WN2–4	–	13
64	23:58:00.161	−32:35:33.11	0.51	20.03 0.03	−0.26 0.13	19.41 0.03	−0.09 0.12	0.18	−7.81	−9.20	(not WR?)	D121	15
65	23:58:00.186	−32:33:22.03	0.81	–	–	22.47 0.08	–	0.18		−6.14	(WC?)	–	12
66	23:58:00.222	−32:34:01.40	0.64	–	–	20.26 0.07	−0.27 0.12	0.18		−8.35	(WN?)	–	12
67	23:58:00.239	−32:34:46.21	0.52	21.07 0.06	0.09 0.11	20.66 0.03	−0.23 0.08	0.18	−7.45	−7.95	(WN?)	D127	13
68	23:58:00.511	−32:34:10.54	0.62	20.52 0.06	0.03 0.12	20.12 0.04	−0.21 0.05	0.18	−8.00	−8.49	(WN?)	D124	12
69	23:58:00.718	−32:35:48.95	0.57	20.92 0.05	−0.17 0.05	20.06 0.04	–0.78 0.06	0.15	−7.49	−8.43	WN2–4	–	15
70b	23:58:00.933	−32:33:56.59	0.68	20.63 0.04	–0.21 0.17	20.15 0.04	–0.14 0.08	0.18	−8.36	−8.81	⊐WN2–4	D129	12
70a	23:58:00.984	−32:33:56.22	0.69	20.16 0.04	–0.12 0.14	19.80 0.02	−0.18 0.16	0.18	−7.89	−8.46		D129	12
71	23:58:01.194	−32:33:37.19	0.77	20.31 0.06	−0.06 0.15	20.04 0.05	−0.37 0.08	0.18	−8.21	−8.57	(WN?)	D130	12
72	23:58:01.720	−32:33:46.37	0.75	22.37 0.10	−0.23 0.10	21.17 0.03	−0.77 0.45	0.13		−7.24	WN2–4	D131	12
73a	23:58:06.631	−32:34:53.44	0.79	n/a	n/a	20.21 0.08	−0.25 0.40	0.12	n/a	−8.18	WC4	D132	17
73b	23:58:06.666	−32:34:51.68	0.80	n/a	n/a	19.53 0.04	−1.37 0.05	0.12	n/a	−8.86	(WC?)	D132	17
74a	23:58:06.898	−32:34:56.17	0.81	n/a	n/a	20.82 0.04	−0.39 0.06	0.18	n/a	−7.79	(WN?)	D132	17
74b	23:58:07.005	−32:34:55.94	0.81	n/a	n/a	21.18 0.03	−0.12 0.03	0.18	n/a	−7.43	(not WR?)	D132	17
Q2358–32	23:58:02.881	−32:36:14.03		20.79 0.01	0.20 0.02	20.38 0.01	−0.62 0.08				QSO	–	19

[1] m_{5100} photometry
[2] m_B photometry
[3] Upper limit since weak nebular Hβ emission

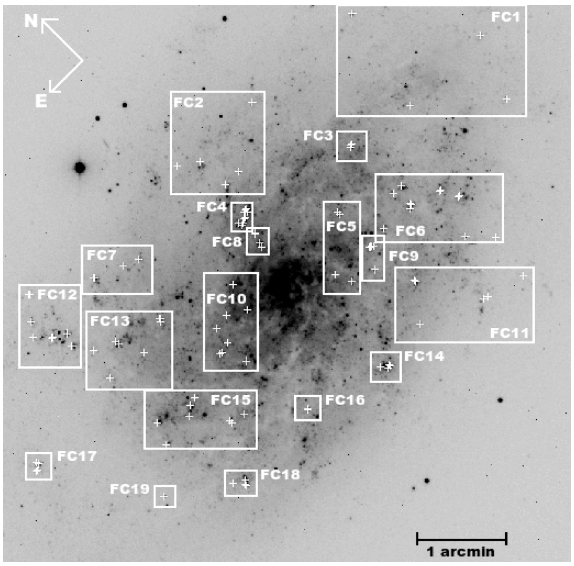

Figure 2. 6.8 × 6.8 arcmin^2 VLT/FORS1 He II finding chart showing the location of WR candidates. More detailed, individual finding charts can be found online (see supporting information).

3 NEBULAR ANALYSIS

In this section, we determine the nebular properties of individual H II regions in NGC 7793 and determine an average extinction and metallicity. We compare our results to previous work and discuss the presence of a metallicity gradient in NGC 7793.

3.1 Interstellar extinction

70 per cent of the 42 MOS spectra reveal nebular Balmer line emission which we can use to derive the interstellar extinction of the region. Examples are presented in Fig. 3. We used the emission-line fitting (ELF) routine within the STARLINK package DIPSO to fit Gaussian profiles to the Balmer lines in the extracted spectra. Using Case B recombination theory (Hummer & Storey 1987), we assumed an electron density of $n_e \sim 100\,\mathrm{cm}^{-3}$ and temperature $T_e \sim 10^4$ K together with a standard Galactic extinction law (Seaton 1979) to estimate the interstellar extinction from the observed Hα/Hβ line

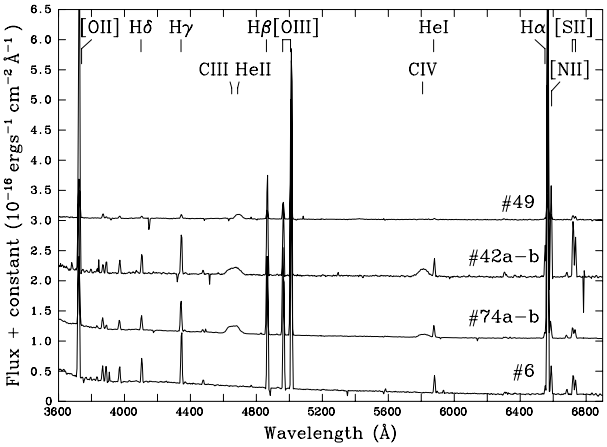

Figure 3. VLT/FORS spectroscopy showing examples of nebular and WR line features for sources in NGC 7793. In sources 42 and 72 the C III, He II and C IV emission are WR features. For clarity, spectra are successively offset by 1×10^{-16} erg s^{-1} cm^{-2} Å^{-1}.

ratio. Observed and extinction corrected nebular line fluxes are shown for six H II regions in Table 3 , while a complete catalogue of the 29 H II regions (including the nucleus) is available online (see Supporting Information).

We note that we do not formally correct for the underlying stellar Balmer line absorption, quantified by McCall (1982) to be of the order of 2 Å for Hα and Hβ. This results in a larger percentage error for nebular lines with a small equivalent width (EW). Mazzarella & Boroson (1993) conclude that the underlying absorption causes their extinction to be overestimated by 15–20 per cent. Our nebular lines have an EW(Hβ) in the range 10–100 Å so we estimate errors of ∼2–20 per cent (0.01–0.1 mag) on our $E(B-V)$ values. Sources with larger errors are highlighted in Table 2 with quoted $E(B-V)$ values representing upper limits.

Excluding a few outliers with unphysical extinction measurements, derived values range from the Galactic foreground extinction of $E(B-V) = 0.019$ mag (Schlegel, Finkbeiner & Davis 1998) to 0.319 mag. The average is $E(B-V) = 0.179 \pm 0.024$ mag. Our values are much lower than those found by Chun (1983) who find extinctions in the range $E(B-V) = 0.56$–0.88 mag. However, they are more consistent with Webster & Smith (1983) who measure c(Hβ) $= E(B-V)/0.7 = 0.23$–0.61. Unfortunately, there are no H II regions common to all three samples so a direct comparison cannot be made.

3.2 Metallicity

Elemental abundances are best determined from the weak line method described in Osterbrock (1989). This method relies on accurate determination of the temperature of the region from the weak [O III] λ4363 line and is preferable to strong line methods. Unfortunately, the [O III] λ4363 line is marginally detected in only four of the H II regions observed in our MOS spectra, and moreover the detection is below the 3σ level. As a result, the errors associated with the derived temperatures are too high to allow reliable abundance determinations and so we resort to strong line methods.

By calculating both the I([N II] λ6584)/I(Hα) and I([O III] λ5007)/I(Hβ) ratios, we can use the N2 and O3N2 indices derived in Pettini & Pagel (2004) to determine the abundance of H II regions within NGC 7793 to ±0.2 dex. Metallicities of the H II regions ranges from log(O/H)+12 = 8.19 to 8.69 with an average value of log(O/H) + 12 = 8.44 ± 0.24 (see Table 4). This is consistent with previous estimates of log(O/H)+12 = 8.54 for NGC 7793 by Pilyugin, Vílchez & Contini (2004), but is somewhat lower than log(O/H)+12 = 8.7 quoted in O'Halloran, Satyapal & Dudik (2006). This difference may be explained by the presence of metallicity gradient of approximately

$$\log \frac{\mathrm{O}}{\mathrm{H}} + 12 = (8.61 \pm 0.05) - (0.36 \pm 0.01)\frac{r}{R_{25}}$$

as shown in Fig. 4. Webster & Smith (1983) also found evidence of a metallicity gradient in NGC 7793 with 12+log(O/H) = 8.23–8.96.

4 THE WOLF–RAYET POPULATION OF NGC 7793

WR stars are relatively straightforward to identify and classify from optical spectra due to their strong, broad emission lines. WN stars are dominated by He II λ4686, while WC stars are dominated by C III λ4650 and C IV λ5801–12 and oxygen-rich (WO) stars by O VI λ3811–34. Individual WC stars possess much larger EWs than WN stars, therefore, allowing for dilution by neighbouring stars

Table 3. Observed, F_λ, and dereddened, I_λ, nebular fluxes of H II regions in NGC 7793, relative to Hβ. The final row lists Hβ fluxes in units of $\times 10^{-15}$ erg s^{-1} cm^{-2}. The complete version of this table is available online (see supporting information).

λ(Å)	ID	1		3		4		5		7a–b		9	
		F_λ	I_λ	F_λ	I_λ	F_λ	I_λ	F_λ	I_λ	F_λ	I_λ	F_λ	I_λ
3727	[O II]	254	306	251	287	547	612	171	199	296	335	154	154
4343	Hγ	38	42	44	47	43	53	40	43	41	43	53	53
4861	Hβ	100	100	100	100	100	100	100	100	100	100	100	100
4959	[O III]	45	44	74	73	73	72	92	91	29	29	22	22
5007	[O III]	138	135	221	217	239	236	272	266	86	84	66	66
6563	Hα	365	290	340	288	331	288	352	290	338	289	232	192
6583	[N II]	40	31	34	29	72	63	21	17	56	48	41	41
6716	[S II]	27	21	28	23	42	36	15	12	38	32	18	18
6731	[S II]	19	15	20	17	34	29	10	8	27	23	7	7
4681	Hβ	0.901	1.85	2.92	4.89	0.104	0.161	2.08	3.80	4.39	7.15	0.308	0.308

Table 4. Deprojected distances from the centre of the galaxy, N2 and O3N2 derived metallicities for H II regions within NGC 7793. The error on the average value is ±0.24 dex.

Source ID	r/R_{25}	I([N II]) I(Hα)	log(O/H) + 12[1]	I([O III]) I(Hβ)	log(O/H) + 12[2]	log(O/H) + 12 mean
1	0.88	0.109	8.35	1.35	8.38	8.37
3	0.95	0.100	8.33	2.18	8.30	8.32
4	0.62	0.218	8.52	2.36	8.40	8.46
6	0.65	0.059	8.20	2.66	8.20	8.20
7ab	0.49	0.165	8.45	0.84	8.50	8.48
9	0.55	0.176	8.47	0.64	8.55	8.51
10	0.40	0.115	8.36	3.82	8.25	8.30
11a-c	0.46	0.164	8.45	1.46	8.43	8.44
14	0.37	0.067	8.23	2.24	8.24	8.24
16	0.70	0.088	8.30	4.18	8.19	8.25
20	0.27	0.399	8.67	–	–	8.67
22a-c	0.27	0.116	8.37	1.56	8.37	8.37
23	0.55	0.166	8.46	3.26	8.32	8.39
26	0.17	0.459	8.71	0.68	8.68	8.69
27	0.49	0.220	8.53	1.42	8.47	8.50
34	0.19	0.256	8.56	0.97	8.55	8.55
35	0.31	0.280	8.58	0.94	8.56	8.57
36	0.17	0.233	8.54	0.74	8.57	8.56
37	0.56	0.145	8.42	1.37	8.42	8.42
39	0.15	0.158	8.44	–	–	8.44
42ab	0.54	0.234	8.54	1.80	8.45	8.49
46	0.51	0.175	8.47	1.42	8.44	8.45
47	0.25	0.231	8.54	0.70	8.58	8.56
49	0.55	0.178	8.47	5.45	8.25	8.36
50a-c	0.35	0.548	8.56	1.28	8.61	8.58
62	0.72	0.139	8.41	3.33	8.29	8.35
69	0.57	0.082	8.28	4.11	8.19	8.23
Average		0.19				8.44 ± 0.24

[1]N2
[2]O3N2

(see Section 5.2), this can result in an observational bias towards WC stars (Massey & Johnson 1998; Crowther et al. 2003).

From our 74 candidate WR regions identified from the continuum-subtracted λ 4684 image we obtained spectra of 39. For these sources, the He II/C III excess ranged from +0.1 to −1.5 mag. From the 39 spectra, 33 revealed WR features ($\geq 3\sigma$), while six showed solely nebular lines. This 85 per cent detection rate is consistent with spectroscopy of NGC 1313 by Hadfield & Crowther (2007), who found 70 of their 82 candidates to exhibit WR features. The sources in NGC 7793 that do not contain WR emission have $m_{4684} - m_{5100} = -0.22 \pm 0.1$ mag. It is likely that these false candidates arise from the formal photometric errors of 0.1–0.2 mag (see Section 2.3). We note that from the subregions found using higher spatial resolution broad-band imaging we obtained spectra in 43 cases, 35 of which have WR features.

Fig. 5 compares the photometric He II excess to the spectroscopic excess for all of our spectroscopic sources. The spectroscopic excess was calculated from the convolution of synthetic spectra with

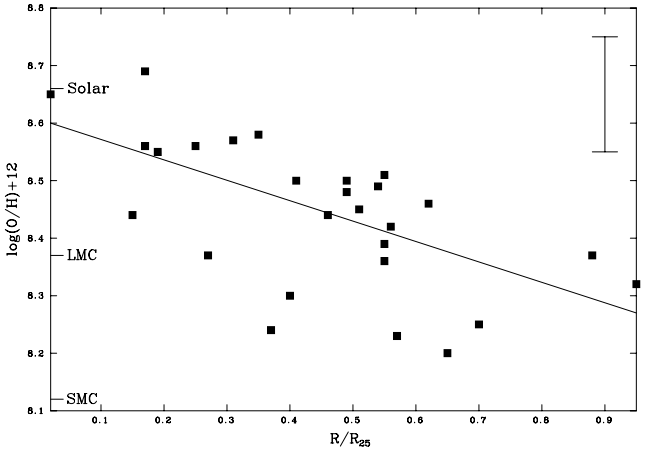

Figure 4. Comparison of the metallicity of H II regions within NGC 7793 relative to their position from the centre of the galaxy. Typical error bars are shown (0.2 dex).

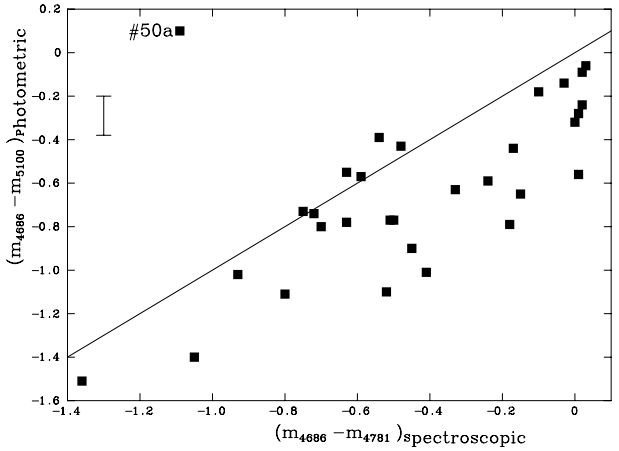

Figure 5. Plot of spectroscopic magnitudes against photometric magnitudes for sources in NGC 7793 of which we have spectra. Outliers indicate unreliable magnitudes determined from photometry. Photometric errors are shown, spectroscopic errors are not due to large variance.

appropriate narrow-band filters. Outliers from the trend indicate that the magnitude derived from photometry is unreliable. There is reasonable agreement with the exception of source 50a owing to severe crowding.

Using the DIPSO ELF routine, the flux and FWHM of the emission lines could be measured; these are presented in Table 5. Typical errors on the line flux measurements were ∼5 per cent for strong lines such as He II λ4686 and C IV λ5808, but were significantly higher, ∼20 per cent, for weaker lines such as N V λ4603 and He II λ5411. Given the similar metallicity of NGC 7793 to the LMC, we use line fluxes of LMC WR stars found in Crowther & Hadfield (2006) as a comparison to assess the number of WR stars in each source. A larger WR population would be inferred from Small Magellanic Cloud (SMC) WR line luminosities, while the reverse would be the case using Milky Way templates.

4.1 WN subtypes

Using the classification scheme derived by Smith, Shara & Moffat (1996), we can divide WN stars into early (WNE, WN2–4), mid (WN5–6) and late (WNL, WN7–9) categories, which are dominated by N V λ4603−20, N IV λ4058 + N III λ4636−4641 and N III λ4634−41, respectively. If only He II λ4686 was detected, we assumed a WNE subtype based on the broad-line emission (FWHM(WNE) = 20–60 Å), relative to narrower emission-line (FWHM(WNL) < 20Å) seen in late-type WR stars (Crowther & Smith 1997). From comparison with WR luminosities in the LMC (Crowther & Hadfield 2006), we can estimate the number of WN stars that are responsible for the He II λ4686 emission. Figs 6 (a) and (b) show examples of WNE and WNL stars in NGC 7793, respectively, together with the spectra of template stars in the LMC. From all our spectra, we estimate ∼27 WN stars present within 13 regions (14 subregions), of which the majority (>80 per cent) are WNE stars, which is a similar fraction to the LMC (Breysacher, Azzopardi & Testor 1999).

4.2 WC subtypes

The larger EW of emission lines in WC stars makes them easier to detect compared to WN stars (Massey & Johnson 1998). Smith, Shara & Moffat (1990) produced a quantitative classification scheme for WC stars based on the de-reddened line flux ratio of C IV λ5808/C III λ5696 and C III λ5696/O V λ5590. This was further refined by Crowther, De Marco & Barlow (1998) whose subtype classification we use here. For sources 36, 47 and 59, we determine a WC6 subtype, for other sources where C III λ5696 is present the detection is below the 3σ level. Hence, we cannot determine a more accurate subtype than WC4–6 in such cases. No late-type WC stars are found in NGC 7793, again consistent with the LMC (Breysacher et al. 1999) and other metal-poor galaxies.

Figs 6(c) and (d) show examples of a WC4 and WC6 spectra, respectively, and are again compared to LMC template WR stars from Crowther & Hadfield (2006). The WC stars lie within bright regions arising from unrelated OB stars in the source. We estimate a total of ∼25 WC stars from 20 sources spectroscopically observed.

4.3 Composite WN and WC spectra

Of the 33 regions displaying WR signatures only source 34 displays the spectral signature of both WN and WC stars. In view of the large Hα flux of this region, which corresponds to ∼20 O7V stars (GHR 3; Table 7), we shall assume that the WN stars present are WN5-6 stars since this subtype is seen to dominate in young bright H II regions (Crowther & Dessart 1998). From spectral line fitting, using LMC template stars, we estimate that three WN5–6 and three WC4 stars are located in this region as shown in Fig. 7. In total, from spectroscopy we find 52 WR stars in NGC 7793, 10 per cent of which are located within the region of candidate 34 (see Section 8).

4.4 WC line widths

Schild, Smith & Willis (1990) have studied the WC content of M33 revealing a correlation between line width (C IV λ5808 FWHM) and galactocentric distance (r/R_{25}), supported by results of Canada–France–Hawaii Telescope (CFHT) spectroscopy in Abbott et al. (2004). In Fig. 8, we re-produce Fig. 6 from Abbott et al. (2004) together with unpublished M33 William Herschel Telescope (WHT)/Wide-field Fibre Optic Spectrograph (WYFFOS) data taken in 1998 August, plus our own NGC 7793 observations. Indeed,

Table 5. WR features, observed flux (F_λ) and extinction corrected luminosities (L_λ) based on a distance of 3.91Mpc and $E(B-V)$ values given in Table 2. Values in the parentheses indicates a less secure detection ($<3\sigma$). Number of WR stars are based on the line luminosities for one WR star from Crowther & Hadfield (2006).

	$F_\lambda(\times10^{-16}$ erg s^{-1} cm$^{-2})$						$L_\lambda(\times10^{36}$ erg s$^{-1})$			
No. of source	*F*(N v/N iii) 4603-4641	*F*(C iii) 4647-4651	*F*(He ii) 4686	*F*(He ii) 5411	*F*(C iii) 5696	*F*(C iv) 5808	*L*(He ii) 4686	*L*(C iv) 5808	WR subtype	*N*(WR)
4	–	8.95	–	–	–	4.54	–	1.17	WC4–6	1
8		–	2.46	–	–	–	0.84	–	WN10	1
9	4.07	–	8.00	0.70	–	–	2.72	–	WN8	4
10	1.52	–	12.7	1.78	–	–	4.14	–	WN2–4b	4
14	–	5.73	–	–	–	4.51	–	1.82	WC4	1
16	–	–	6.03	–	–	–	2.77	–	WN2–4	3
20	–	12.04	–	–	–	7.56	–	2.22	WC4	1
23	–	11.59	–	–	–	5.81	–	1.49	WC4	1
24	–	11.2	–	–	(0.84)	3.46	–	0.97	WC4	1
25	–	2.27	–	–	–	1.55	–	0.46	WC4	1
26	–	4.14	–	–	(0.30)	1.52	–	0.43	WC4–6	1
27	–	4.53	–	–	–	3.77	–	1.11	WC4	1
34	(5.87)		19.0	–	–	19.8	10.5	8.43	WN5–6:WC4	3:3
35	–	4.43	–	–	–	2.08	–	0.48	WC5–6	1
36	–	14.21	–	–	0.98	7.15	–	2.68	WC6	1
37	–	15.43	–	–	(0.30)	7.87	–	2.03	WC4–6	1
39	–	–	3.17	–	–	–	1.08	–	WN2–4	2
42ab	–	13.90	–	–	–	11.7	–	4.59	WC4	2
43	–	7.25	–	–	(0.20)	3.25	–	0.95	WC4–6	1
45	–	4.38	–	–	(0.37)	2.17	–	0.64	WC4–6	1
46	–	35.56	–	–	–	12.7	–	3.22	WC4	2
47	–	18.94	–	–	0.38	7.23	–	2.03	WC6	1
49	0.62	–	4.73	6.06	–	–	1.61	–	WN3	2
50a	–	6.85	–	–	–	3.62	–	1.28	WC4	1
55	–	6.57	2.35	–	–	3.67	–	1.08	WC5–6	1
56	1.39	–	1.27	0.66	–	–	0.43	–	WN2–4	1
59	–	5.76	–	–	0.33	4.14	–	1.21	WC6	1
62	–	–	6.10	0.69	–	–	1.43	–	WN2–4	2
63	–	–	2.65	0.34	–	0.87	0.18	0.26	WN2–4	1
69	0.87	–	4.77	–	–	–	1.44	–	WN2–4	2
70ab	–	–	1.56	–	–	–	0.53	–	WN2–4	1
72	0.36	–	1.33	–	–	–	0.74	–	WN2–4	1
73a	–	13.93	–	–	–	4.44	–	1.11	WC4	1

there is a deficit of broad-lined WC4–6 stars at low galactocentric distances.

The combined sample of WC stars, in M33 and NGC 7793, possess stronger winds in the moderately metal-rich inner, compared to the metal-poor outer regions. Crowther et al. (2002) argued that the difference between WC subtypes in metal-poor and metal-rich galaxies was metallicity-dependent winds. Metal-poor regions in galaxies exhibit (broad-lined) WC4 stars, while metal-rich regions possess (narrow-lined) WC8–9 stars. In between these extremes, the dominant subtype would naturally be ∼WC6 subtypes as is the case for the inner regions of NGC 7793 and M33. We would expect broad-line sources to have fast winds which is not consistent with their metal-poor location. The physical explanation behind this apparent anti-correlation of metallicity and wind velocity is not understood.

For the WCE stars, there appears to be a correlation between the FWHM of C iv λ5808 and the relative strength of the C iv λ5808/C iii λ4650 lines, with narrower lines having weaker C iv λ5808. The WC4–6 stars in NGC 7793 appear to span a larger range than the WC4 stars in the LMC (Crowther & Hadfield 2006). This is presented in Fig. 9 and would be a natural consequence of somewhat later (WC5–6) subtypes for most NGC 7793 WC stars.

5 COMPARISON OF VLT AND *HST* DATA

In this section, we consider the advantages of space-based observations in identifying WR sources in galaxies beyond the Local Group. We consider the case of the LMC to assess what fraction of known LMC WR stars would have been detected at the distance of NGC 7793.

5.1 Spatial resolution

33 of our 39 spectra showed WR features for which we have obtained photometry from ground-based VLT images. However, crowding and the spatial resolution of He ii ground-based images cause these sources to be contaminated by stars along similar lines of sight, or stars within the same cluster. For NGC 7793 at a distance of 3.91 Mpc (Karachentsev et al. 2003), the spatial resolution of our ground-based He ii images is 1.3 arcsec corresponding to a physical scale of ∼25 pc compared to 0.1 arcsec resolution, or ∼2 pc, with the *HST*. The dramatic improvement of space-based images is demonstrated in Fig. 10. We can take advantage of archival *HST* imaging of NGC 7793 (Section 2.2) to more accurately locate the WR source and determine a more robust magnitude. Unfortunately, not all of NGC 7793 have been observed with the ACS/WFC using

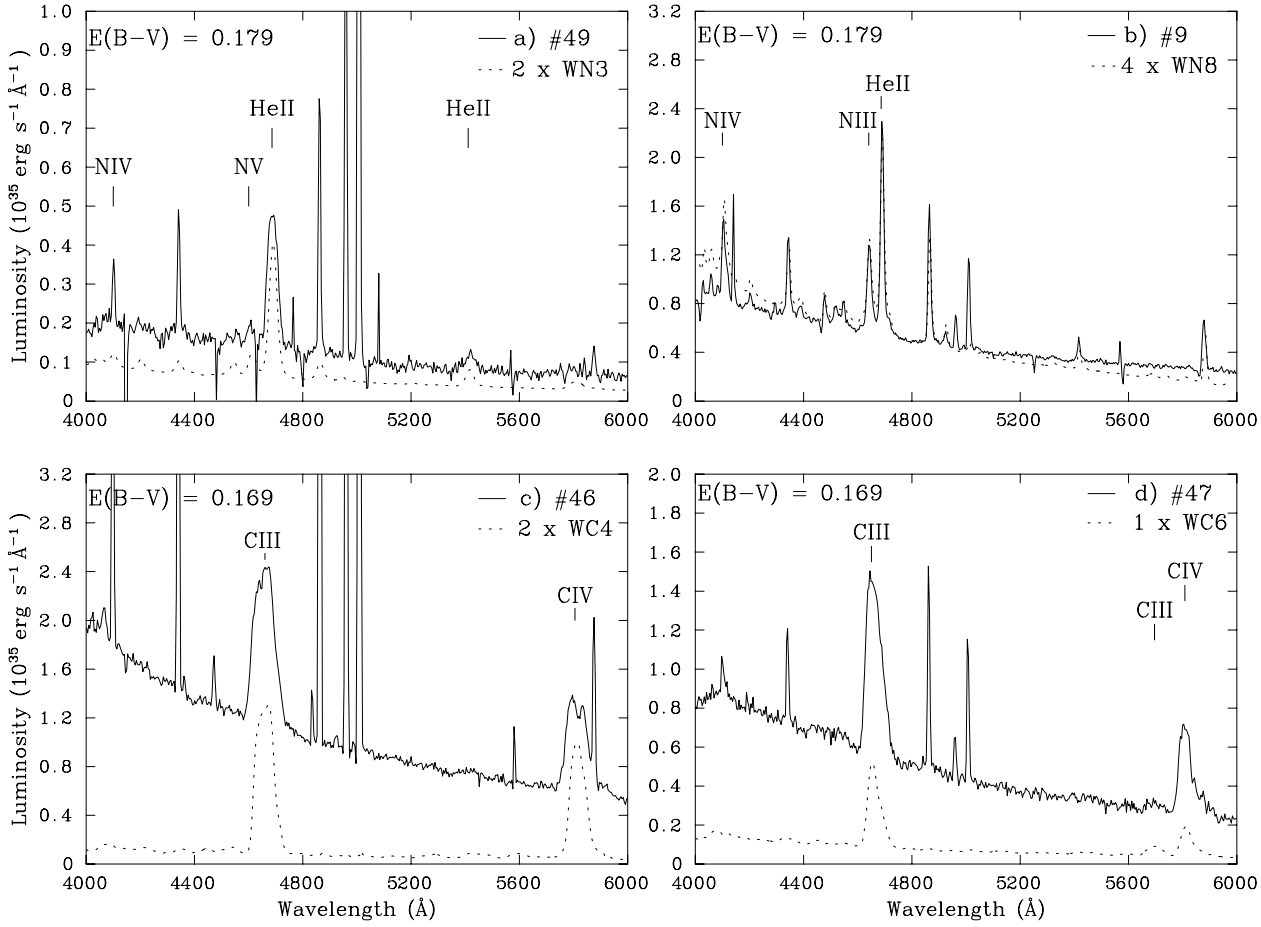

Figure 6. Extinction and distance corrected spectra of WN stars [(a) and (b)] and WC stars [(c) and (d)] in NGC 7793 (solid lines) compared to templates of LMC WR stars (dashed lines).

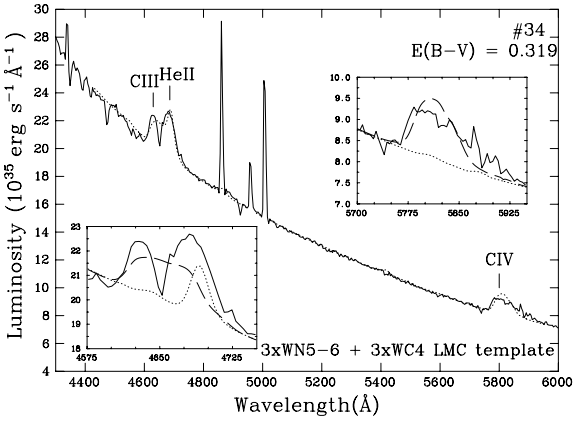

Figure 7. Source #34 in NGC 7793. Solid line is VLT/FORS data. Dotted line (main plot) is LMC template of 3 WN5-6 stars and 3 WC4 stars. Inset show contributions from WC4 stars (dashed line) and WN5-6 stars (dotted line).

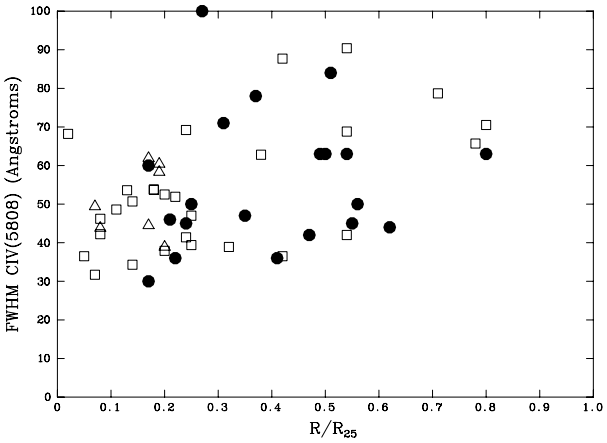

Figure 8. FWHM C IV λ5808 increases with r/R_{25} for WC4-6 stars in NGC 7793 and M33. NGC 7793 data (circles) are plotted with unpublished WHT/WYFFOS (empty squares) and CFHT/MOS data (empty triangles) for M33 (Abbott et al. 2004).

the F555W filter. 10 of our candidates lie within the ACS pointing (recall Fig. 1).

We are able to spatially resolve the WR source for six of the 10 cases using offsets from nearby point sources to the peak of the He II emission identified from the archival VLT images. Two examples are shown in Fig. 10. Table 6 shows that the measured *HST* magnitudes for five WR sources are 0.4–1.4 mag fainter, arising from severe crowding in the VLT images. Source 36 was not identified by DAOPHOT in the VLT *V*-band image, although an *HST* magnitude can be determined. Sources 8 and 34 can only be partially resolved

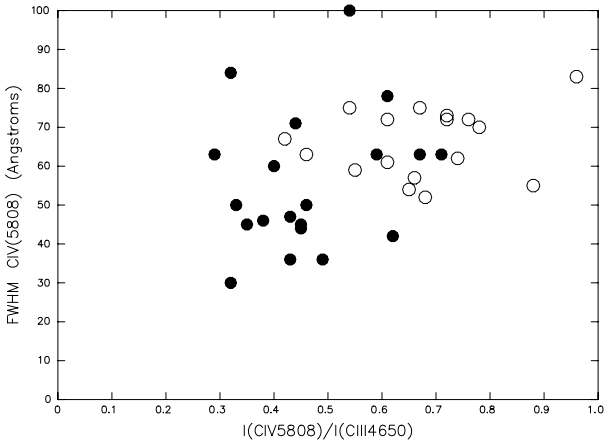

Figure 9. FWHM C IV λ5808 increases with I(C IVλ5808/C III λ4650) line ratio for WC4–6 stars. NGC 7793 data (filled circles) are compared to LMC WC4 data (empty circles).

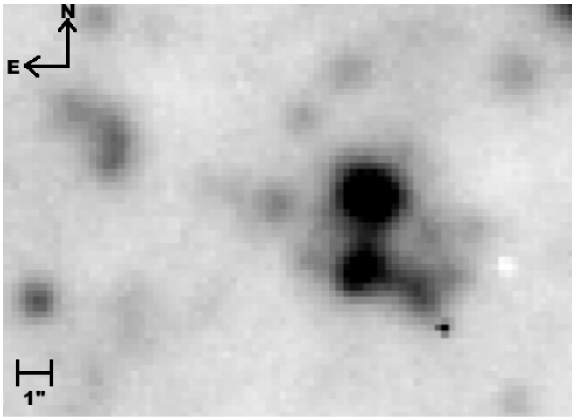

(a)

(b)

Figure 10. Comparison of (a) ground-based λ 4684 VLT/FORS1 imaging with (b) space-based *HST*/ACS F555W imaging. The image is ∼15 × 10 arcsec^2 (300 × 200 pc). From archival *HST* images, we are able to locate the WR source more accurately than using ground-based data.

from the compact host cluster in the *HST* image, making little difference to the observed magnitude. The final two WR sources (24 and 26) are located in dense clusters, so despite the superior spatial resolution of *HST*, we cannot identify the individual WR source. If *HST*/ACS F555W imaging were available for all 74 sources in NGC 7793, magnitudes would typically be 1 ± 0.5 mag fainter than those quoted in Table 2.

Table 6. *HST* F555W magnitudes compared with VLT *V*-band magnitudes for WR sources in NGC 7793. The *HST* magnitudes are fainter due to an increased spatial resolution so the multiple objects are no longer included in the aperture. The RA and Dec. values correspond to the *HST* position of the WR source.

ID	RA J2000	Dec. J2000	m_V mag	m_{F555W} mag	$m_{F555W} - m_V$ mag
4	23:57:37.133	−32:35:01.33	22.48	23.91	1.43
8	23:57:39.550	−32:37:24.32	20.97	20.78	−0.19[a]
10	23:57:40.809	−32:35:36.21	20.18	21.43	1.25
14	23:57:41.421	−32:35:35.49	21.27	22.28	1.01
20	23:57:45.325	−32:36:05.17	22.50	22.90	0.4
24	23:57:46.647	−32:36:00.28	21.99	–	[b]
25	23:57:46.787	−32:34:05.80	21.81	22.60	0.79
26	23:57:47.049	−32:35:48.11	22.49	–	[b]
34	23:57:48.830	−32:34:53.10	18.07	18.09	0.02[a]
36	23:57:49.037	−32:34:57.41	–	23.10	–

[a]WR source only partially resolved from host cluster
[b]WR source is not resolved from host cluster

5.2 Completeness compared to the LMC

We can investigate the completeness of our NGC 7793 survey by degrading observations of a nearby galaxy, that has been completely surveyed for WR stars, to the required resolution. We use ground-based Digitized Sky Survey (DSS)[1] images of the LMC, which lies at a distance of ∼50 kpc (Gibson 2000), to assess the role played by nearby sources on the detection limit for WR stars for a sample of the LMC WR stars listed in Breysacher et al. (1999).

Fig. 11(a) shows the distribution of M_{4684} and $m_{4781} - m_{4684}$ for WR stars in the LMC. Typical broad-band magnitudes of single LMC WR stars are $M_V = -3$ to -7 mag.

We have obtained synthetic narrow-band magnitudes for LMC WR stars from spectrophotometric observations of Crowther & Hadfield (2006) and Torres-Dodgen & Massey (1988). We find $m_{4781} - m_{4684} = 0.1$–$1.8$ mag for WN stars and 0.4–2.4 mag for WC stars. WR sources exceeding $M_{4684} = -9$ mag are clusters containing both O stars and WR stars. For example, R136 (Brey 82) is the youngest, brightest cluster in the LMC (Massey & Hunter 1998), Brey 34 is a WN star with a B supergiant companion (Dopita et al. 1994), whilst Brey 65 is a star cluster hosting a WN star (Walborn et al. 1999). The He II emission from the WR stars within these clusters/binaries has been severely diluted by the companion stars; hence, a relatively small excess is detected. Nevertheless, the majority of the WR stars detected in the LMC can be resolved into single stars.

However, if the LMC were located at a similar distance to NGC 7793, then a higher percentage of the WR sources would be blended with the surrounding stars if they were observed at the same spatial resolution as our archival VLT/FORS imaging. Would

[1] The Digitized Sky Surveys were produced at the Space Telescope Science Institute under US Government grant NAG W-2166. The images of these surveys are based on photographic data obtained using the Oschin Schmidt Telescope on Palomar Mountain and the UK Schmidt Telescope. The plates were processed into the present compressed digital form with the permission of these institutions.

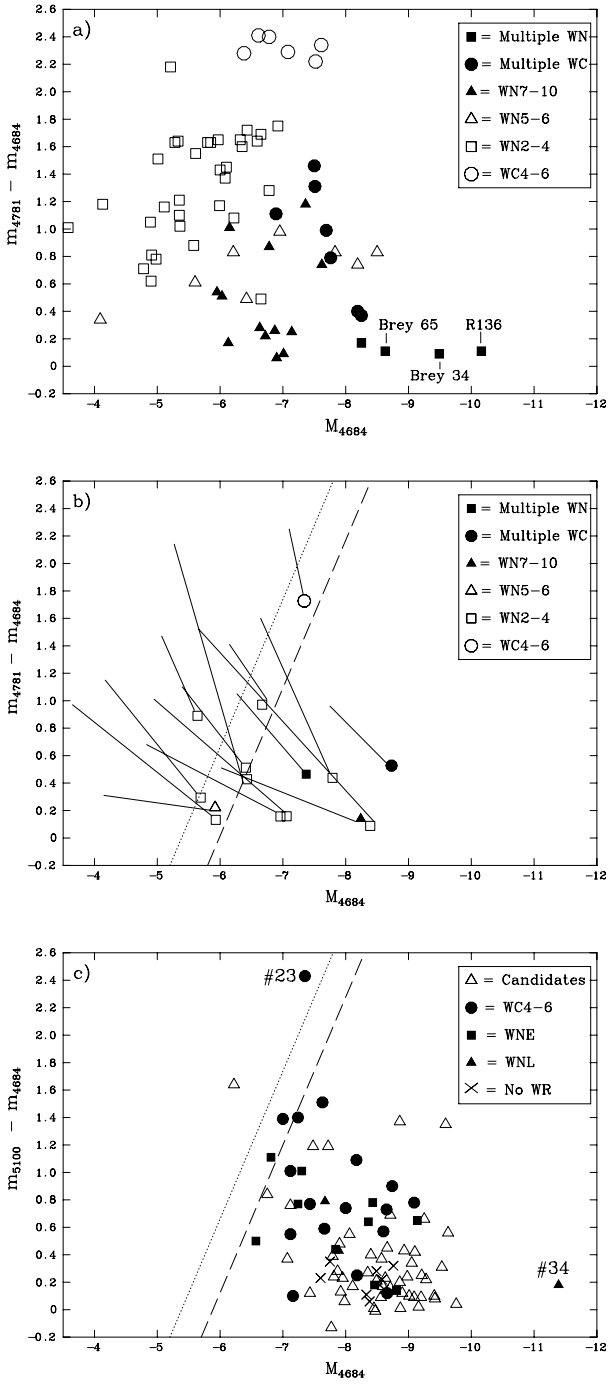

Figure 11. Comparison of $\lambda_c = 4684$ excess emission versus M_{4684} for (a) WR stars in the LMC, (b) a subset of the LMC WR population at a distance of 4 Mpc accounting for the contribution of sources within 1 arcsec (20 pc) and (c) NGC 7793. The solid lines in (b) show the photometric shift arising from an increased aperture size. The diagonal lines in (b) and (c) indicate our 100 per cent (dashed) and 50 per cent (dotted) detection limits. Each sample is split into different subtypes.

the WR emission still be observed, or would it be diluted by surrounding stars to the point that it was no longer detectable?

To address this question, we consider the location of a representative sample of 15 WR stars in the LMC to investigate the effect of a degraded resolution. 1 arcsec corresponds to a spatial scale of ∼0.25 pc at the distance of the LMC versus ∼20 pc for NGC 7793. We have used DSS images to determine how the photometric properties would alter if the surrounding stars were combined with the WR star.

Fig. 11(b) shows the resulting photometry of the He II excess and absolute magnitude of this subset of WR stars in the LMC at a distance of 4 Mpc. The solid lines indicate the shift of the WR stars to the lower right of the figure. Taking into account our formal completeness limit of $M_{4684} \sim -5.8$ mag for NGC 7793, and assuming that we include only sources with $M_{4781} - M_{4684} \geq 0.1$ mag, we would detect at least 80 per cent of the WR stars in the LMC in our VLT imaging survey. Moreover, our 50 per cent detection limit includes all but one of the LMC WR stars in our sample. Fig. 11(b) also shows that there is a bias towards WC stars (Massey & Johnson 1998), such that we would most likely have detected the overwhelmingly majority of the LMC WC stars at 4 Mpc (See Section 8). Fig. 11(c) shows the photometric absolute magnitude and He II excess emission for the WR sources in NGC 7793, with the diagonal line representing the 50 per cent and 100 per cent completeness limits (recall Section 2.3).

6 GIANT H II REGIONS

NGC 7793 contains 132 catalogued H II regions (Davoust & de Vaucouleurs 1980). Using appropriate aperture radii (r_{ap}), we have measured the net Hα flux for the brightest H II regions, limiting our sample to those which exceed $Q_0 > 10^{50}$ photon s^{-1}, formally defined as the GHRs in Conti, Crowther & Leitherer (2008). From comparison with the Cerro Tololo Inter-American Observatory (CTIO) images used in Kennicutt et al. (2008) there are four additional GHRs in NGC 7793 beyond the field of view of our VLT imaging (recall Fig. 1). Two of these are listed in the Davoust & de Vaucouleurs (1980) catalogue as D47 and D132, while the other two have not been discussed. We add the location of the two other four GHRs to Table 7 as GHR A, B, C and D.

Hα fluxes estimated from observations using the Hα narrowband filter are contaminated by the [N II] λ6583 emission and to a lesser degree by [N II] λ6548. To correct for this, we have determined the [N II] λ6583 contribution from our spectroscopic data, or adopt an average value of I([N II] λ6583)/I(Hα) = 0.19 otherwise. 97 per cent of our I([N II] λ6583)/I(Hα) values are within 1σ (0.2) of the mean value. Webster & Smith (1983) obtain a mean value I[N II] λ6583/I(Hα) = 0.23 from spectroscopy of H II regions, while McCall, Rybski & Shields (1985) find a higher mean value of I([N II] λ6583)/I(Hα) = 0.35 from the average of only three H II regions. After subtracting the continuum, observed fluxes were extinction corrected. Table 7 lists values of $E(B-V)$ and I([N II] λ6583)/I(Hα) for each source.

We have calculated a Hα luminosity of 3.30×10^{40} erg s^{-1} or a SFR ∼ 0.26 M$_\odot$ yr^{-1} (using equation 2 in Kennicutt 1998) for the region surveyed with FORS1 (recall Fig. 1). A more accurate value for the whole galaxy can be made by applying our mean values of $E(B-V)$ and I([N II] λ6583)/I(Hα) to the observed (Hα+[N II] λ6583) flux of Kennicutt et al. (2008). The revised SFR = 0.45 M$_\odot$ yr^{-1}, 50 per cent larger than their SFR ∼ 0.30 M$_\odot$ yr^{-1}, suggesting that emission beyond our Hα survey contributes ∼40 per cent of the total. We note that young H II regions could be visibly obscured, increasing the global SFR. However, NGC 7793 is included in the Spitzer Infrared Nearly Galaxies Survey (SINGS) survey (Kennicutt et al. 2003), for which Prescott et al. (2007) concluded that NGC 7793 has no highly obscured bright H II regions. Therefore, the Hα-derived SFR should reflect the true value.

Table 7. Catalogue of Giant H II Regions (GHRs) in NGC 7793. All luminosities are based on a distance of 3.91 Mpc (Karachentsev et al. 2003). F(Hα) is the continuum subtracted, [N II] λ6583 corrected observed flux. We note that there are ∼4 additional GHII regions within the outer regions of NGC 7793 beyond our VLT/FORS1 Hα surveyed region, two of which are listed in the Davoust & de Vaucouleurs (1980) catalogue. The final two rows relate to our Hα survey region, and global properties for NGC 7793 updated from Kennicutt et al. (2008).

ID	RA J2000	Dec. J2000	r_{ap}^{1} (arcsec)	$E(B-V)$ (mag)	I[N II]/I(Hα)	F(Hα) (erg s^{-1} cm^{-2})	L(Hα) (erg s^{-1})	log Q_0 (s^{-1})	N(O7V)	H II region	WR
GHR 1	23:57:41.166	−32:35:50.89	6.25	0.179	0.19	1.80×10^{-13}	5.00×10^{38}	50.57	37	D13	12ab
GHR 2	23:57:41.237	−32:34:51.45	3.75	0.179	0.16	1.40×10^{-13}	3.89×10^{38}	50.46	29	D14	11a–c
GHR 3	23:57:48.889	−32:34:53.13	3.00	0.319	0.26	8.24×10^{-14}	3.17×10^{38}	50.37	23	–	34[3]
GHR 4	23:57:54.250	−32:33:59.78	4.75	0.242	0.18	9.60×10^{-14}	3.09×10^{38}	50.36	23	D95	46[3]
GHR 5	23:57:43.271	−32:35:49.90	4.75	0.179	0.19	1.03×10^{-13}	2.86×10^{38}	50.33	21	D20	17
GHR 6	23:57:46.711	−32:36:06.69	3.50	0.179	0.19	9.27×10^{-14}	2.58×10^{38}	50.28	19	D36	–
GHR 7	23:57:57.041	−32:36:08.62	4.50	0.179	0.19	8.55×10^{-14}	2.38×10^{38}	50.25	18	D110	53
GHR 8	23:57:56.968	−32:33:48.35	4.25	0.179	0.19	8.08×10^{-14}	2.25×10^{38}	50.22	17	D111	52ab
GHR 9	23:57:50.798	−32:34:17.55	4.25	0.179	0.19	7.72×10^{-14}	2.15×10^{38}	50.20	16	D73	–
GHR 10	23:57:41.416	−32:35:34.74	2.75	0.298	0.07	5.15×10^{-14}	1.89×10^{38}	50.15	14	D15	14[3]
GHR 11	23:57:48.209	−32:36:15.03	2.50	0.179	0.19	6.64×10^{-14}	1.85×10^{38}	50.14	14	D49	–
GHR 12	23:57:51.194	−32:36:48.75	2.75	0.179	0.19	5.76×10^{-14}	1.60×10^{38}	50.07	12	D74	–
GHR 13	23:57:44.744	−32:34:24.99	2.75	0.179	0.19	5.68×10^{-14}	1.58×10^{38}	50.07	12	D27	–
GHR 14	23:57:44.494	−32:35:52.03	3.00	0.119	0.12	6.50×10^{-14}	1.57×10^{38}	50.07	12	D25	22a–c
GHR 15	23:57:48.391	−32:34:34.25	3.00	0.179	0.19	4.93×10^{-14}	1.37×10^{38}	50.01	10	D55	30ab
GHR A	23:57:48.000	−32:33:04.10								D47	–
GHR B	23:58:06.730	−32:34:58.00								D132	73ab
GHR C	23:57:59.967	−32:33:23.84									–
GHR D	23:58:08.807	−32:36:47.68									–
Hα survey (This study)			205.7	0.179	0.19	1.18×10^{-11}	3.30×10^{40}	52.39	2440	SFR = 0.26 M$_\odot$ yr^{-1}	
Hα survey (Kennicutt et al. 2008)				0.179	0.19	2.04×10^{-11}	5.65×10^{40}	52.62	4180	SFR = 0.45 M$_\odot$ yr^{-1}	

[1] Aperture radius

7 A BACKGROUND QUASAR: Q2358-32

Follow-up MOS spectroscopy of one candidate emission-line source displaying a large excess of $m_{4684} - m_{5100} = -0.62$ mag failed to match that expected for a WR star. This source, for which $m_V = 20.79$ mag, was revealed instead to be a background quasar at $z \sim 2.02$ in which C IV λ1548–51 has been redshifted into the λ4684 narrow-band filter. The quasar spectrum is presented in Fig. 12, which we name Q2358-32.

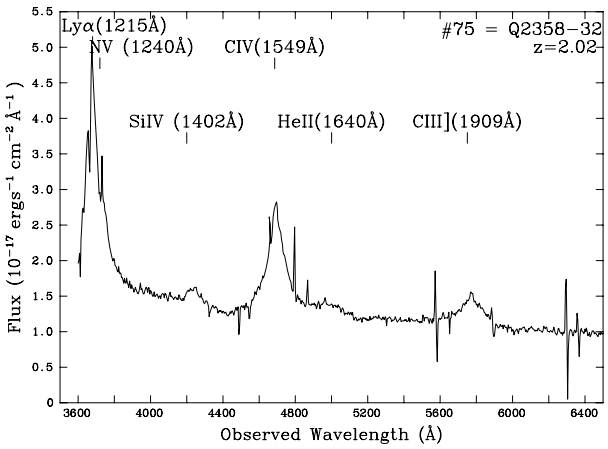

Figure 12. FORS1 spectrum of the background quasar Q2358-32 which lies at $z = 2.02$. This source was picked up in our WR survey because C IV λ1548-51 was redshifted into the $\lambda_c = 4684$ Å narrow-band filter.

NGC 7793 has been observed with the X-ray telescope aboard *ROSAT* (Read & Pietsch 1999). From this survey, the published coordinates of X-ray point source P11 lies ∼20 arcsec from Q2358-32. Although this source has a formal positional error of only 13 arcsec, P11 could plausibly arise from Q2358-32 from inspection of Fig. 1 in Read & Pietsch (1999).

A number of quasars located behind nearby spiral galaxies are known, including a $z = 2.55$ quasar towards NGC 1365 by Bresolin et al. (2005). These have previously been used to investigate the nature of the ISM of the spiral galaxy using the Ca II H and K lines – see Pettini & Boksenberg (1985) and Hintzen et al. (1990). Unfortunately, in the case of Q2358-32, these lines fall on the redshifted Lyα quasi-stellar object emission line; hence, we are unable to calculate the column density of the absorbing gas in this instance (Bowen 1991).

8 GLOBAL WR POPULATION OF NGC 7793 WITH COMPARISON TO NGC 300

8.1 Global WR population of NGC 7793

We confirm the presence of 27 WN and 25 WC stars in NGC 7793 from spectroscopic observations (Table 2). However, to estimate the global number of WR stars in NGC 7793, we may use (a) our narrow-band photometry of remaining candidates and (b) our comparison with the LMC WR population.

On the basis of the distribution of LMC WR stars in Fig. 11(b), we photometrically classify remaining WR candidates in NGC 7793 as follows. We shall assume that sources with $m_{5100} - m_{4684} > +1$ mag are WC subtypes, those for which $+0.2 \leq m_{5100} - m_{4684} \leq +1$ mag

are WN stars, with the remainder either foreground or weak emission-line sources. In reality, there will be instances of WC, WN and spurious candidates in different magnitude bins, but outliers should be relatively few in number. In addition, we uniformly assume that photometric sources host a solitary WR star. A total of 27 WN and eight WC candidates are added to the census in this way, listed in the parentheses in Table 2, suggesting 54 WN and 33 WC stars in total.

Finally, we need to consider the completeness limit of our imaging survey. We estimate that 90 per cent of the WC stars in the region of NGC 7793 surveyed would have been detected, plus 80 percent of the WN stars, on the basis that their intrinsic properties are similar to those in the LMC. Adjusting the WR populations for this effect, we arrive at a total of ∼68 WN and ∼37 WC stars, with $N(\mathrm{WC})/N(\mathrm{WN}) \sim 0.5$ and $N(\mathrm{WR}) = 105$ in total. Our spectroscopic survey has therefore recovered 67 per cent of the estimated WC population and 40 per cent of the estimated WN population. Using the revised global SFR from Section 6, we obtain $N(\mathrm{WR})/N(\mathrm{O7\,V}) \sim 0.025$.

8.2 Comparison between WR populations of NGC 7793 and NGC 300

WR surveys have been conducted within both Local Group galaxies (Massey & Johnson 1998) and beyond. Of those non-Local Group spiral galaxies forming the basis of our supernova progenitor survey, M83 is metal-rich (Hadfield et al. 2005), NGC 1313 is metal-poor (Hadfield & Crowther 2007), leaving the central region of NGC 300 surveyed by Schild et al. (2003) as the ideal comparison galaxy to the present survey of NGC 7793.

NGC 300 is another Sculptor group SA(s)d spiral galaxy, albeit a factor of 2 closer (Gieren et al. 2005). Basic global properties of NGC 300 and NGC 7793 are provided in Table 8 , indicating similar physical sizes and metallicity gradients, although NGC 7793 possesses a factor of 4 higher SFR (Section 6). We also provide a comparison between the WR census of the central region of NGC 300 and the present study. 30 of the 58 WR candidates identified by Schild et al. (2003) have been spectroscopically confirmed by references therein or Crowther et al. (2007). In addition, Crowther et al. (2010) have recently obtained additional MOS spectroscopy of NGC 300 from which five additional WR stars are revealed (7, 10, 21, 37 and 54), to which we add the confirmation of a very late WN star discovered by Bresolin et al. (2009), bringing the total to 20 WN and 17 WC stars, including a couple of composite WN+WC systems (11 and 37). We set a slightly lower λ4684 excess threshold of $m_{4781} - m_{4684} = +0.15$ mag for the remaining photometric candidates in NGC 300 as a result of an improved photometric precision and slightly different continuum filter. Six additional photometric WN stars follow. These bring the total WR census of the inner disk of NGC 300 to $N(\mathrm{WR}) \sim 43$, comprising 26 WN and 17 WC stars, or $N(\mathrm{WC})/N(\mathrm{WN}) \sim 0.65$.

Regarding the O star content of the central region of NGC 300, Crowther et al. (2007) estimated that the WR survey region included ∼78 per cent of the 0.12 $\mathrm{M_\odot\ yr^{-1}}$ global SFR of NGC 300 (Kennicutt et al. 2008). Therefore, $N(\mathrm{WR})/N(\mathrm{O7V}) \sim 0.05$, a factor of 2 higher than NGC 7793. Indeed, the surface density of WR stars in the central region of NGC 300 is also a factor of 2 higher than the entire disk of NGC 7793. This difference may originate in part from the slightly higher metallicity of the inner region of NGC 300, namely log (O/H) + 12 ∼ 8.5, versus an average value of ∼8.4 for NGC 7793.

Table 8. Global properties of NGC 7793 with respect to NGC 300, plus a detailed census of their massive star content within the regions surveyed by Schild et al. (2003) and this study. The values in parentheses include adjustments for sources lacking spectroscopy plus completeness issues for NGC 7793.

Name	NGC 300	NGC 7793
Hubble Type	SA(s)d	SA(s)d
Distance (Mpc)	1.88[a]	3.91[h]
R_{25} (arcmin)	10.9[b]	4.65[b]
R_{25} (kpc)	5.3[b]	5.3[b]
SFR ($\mathrm{M_\odot\ yr^{-1}}$)	0.12[d]	0.45[d,i]
log(O/H) + 12 (centre)	8.57[e]	8.61[i]
Gradient* (dex $\mathrm{kpc^{-1}}$)	−0.08[f]	−0.07[i]
Survey region (kpc)	3.7 × 3.7[c]	9.3 × 7.3[i]
N(O7V)	870[i]	4200[d,i]
N(O)	1300[i]	6250[d,i]
log(O/H) + 12 (mean)	8.5[e]	8.4[i]
WR candidates	58[c,f]	74[i]
N(WN)	20 (26)[c,f,g,j]	27 (68)[i]
N(WC)	17 (17)[c,f,g,j]	25 (37)[i]
N(WC)/N(WN)	0.85 (0.65)[i]	0.93 (0.55)[i]
N(WR)/N(O)	≥0.028 (0.033)[i]	≥0.008 (0.017)[i]
Surface density* (WR $\mathrm{kpc^{-2}}$)	2.7 (3.1)[i]	0.77 (1.6)[i]

[a] Gieren et al. (2005), [b] de Vaucouleurs et al. (1991), [c] Schild et al. (2003), [d] Kennicutt et al. (2008), [e] Urbaneja et al. (2005), [f] Bresolin et al. (2009), [g] Crowther et al. (2007), [h] Karachentsev et al. (2003), [i] this work, [j] Crowther et al. (2010).

8.3 Comparison with evolutionary models

Observations of WR stars in the Local Group have revealed a strong correlation between the ratio of WC to WN stars and WR to O stars as a function of metallicity (Massey 1996). In Fig. 13(a) we provide an updated comparison of $N(\mathrm{WC})/N(\mathrm{WN})$ including spectroscopic and photometry results from our galaxy surveys to date, plus the photometric results of Massey & Holmes (2002). Model predictions are shown from initially rotating (300 $\mathrm{km\,s^{-1}}$) single star models of Meynet & Maeder (2005) plus single and binary models incorporating metallicity-dependent WR winds from Eldridge & Vink (2006). The latter provides a reasonable match to empirical results, although highlights differences between the metal-poor dwarf spiral galaxies (including NGC 7793) and dwarf irregular galaxies (including the LMC).

In order to compare the ratio of WR to O stars with evolutionary predictions, it is necessary to first calculate the number of equivalent O7V stars from nebular Hα luminosities and then attempt to convert this quantity into actual O stars. For the LMC and SMC, we utilize nebular properties from Kennicutt et al. (1995), with Hα luminosities from Lee et al. (2009) used, with the exceptions of IC 10 (Gil de Paz, Madore & Pevunova 2003), NGC 300 and NGC 7793 (recall Section 8.2). These are converted into the number of equivalent O7V stars using equation (2) from Kennicutt (1998) and $Q_0 = 10^{49}\ \mathrm{s^{-1}}$ for O7V stars.

For an instantaneous burst of star formation, $N(\mathrm{O})/N(\mathrm{O7V}) \sim$ 0.7–2 for the first ∼4 Myr at LMC metallicity (Schaerer & Vacca 1998). For continuous star formation, as is the case for galaxies in our sample, we have estimated the conversion factors in two ways. There are ∼1000 O stars in the SMC according to Evans et al. (2004), suggesting $N(\mathrm{O})/N(\mathrm{O7V}) \sim 2$ from its global Hα derived SFR. For the 30 Doradus region of the LMC, the recent VLT-FLAMES Tarantula survey (Evans et al. 2010) reveals ∼400

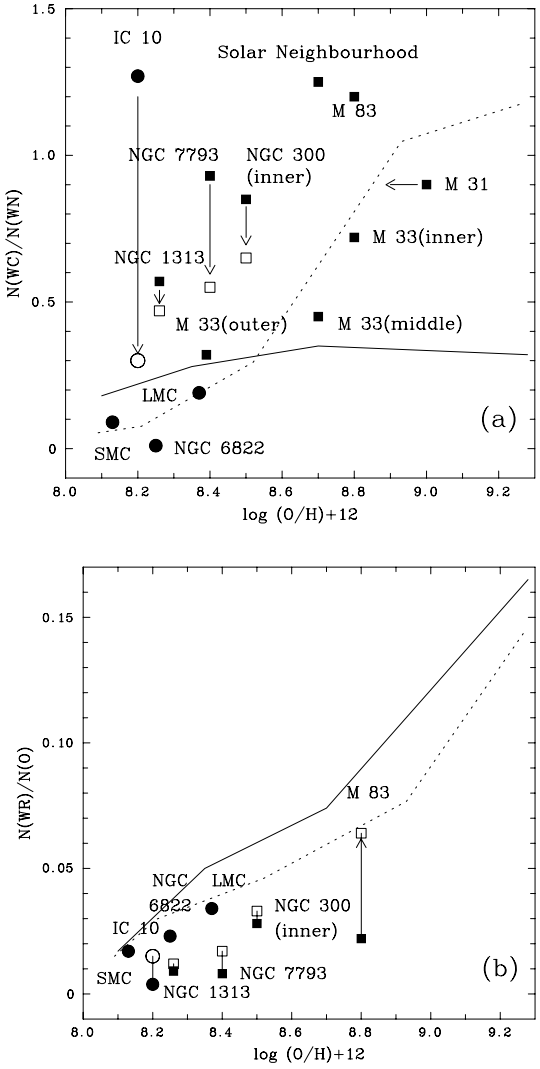

Figure 13. Comparison between (a) N(WC)/N(WN) and (b) N(WR)/N(O) ratios and the oxygen content of nearby spiral (squares) and irregular (circles) galaxies, together with evolutionary predictions from Meynet & Maeder (2005) and Eldridge & Vink (2006). Spectroscopic (filled symbols) and photometric (open symbols) results are shown for NGC 7793, NGC 300, NGC 1313 and IC 10 from the present study, Hadfield & Crowther (2007), Massey & Holmes (2002) and Crowther et al. (2003).

O stars excluding the central R136 ionizing cluster (Crowther & Dessart 1998). 30 Doradus provide a total Lyman continuum ionizing flux of $\sim 10^{52}$ s^{-1}, of which ∼40 per cent is supplied by R136, suggesting N(O)/N(O7V) ∼ 0.7 from 30 Doradus (omitting R136). Fig. 13(b) compares the WR to O ratio for galaxies within our survey and results from the literature (Massey 1996) applying a uniform correction of N(O)/N(O7V) ∼ 1.5 for the whole sample. Once again, evolutionary predictions from Eldridge & Vink (2006) and Meynet & Maeder (2005) are included, with reasonable agreement found for both, albeit highlighting the relatively low WR to O ratio for NGC 7793.

9 SUMMARY

We present the results of a VLT/FORS1 imaging and spectroscopic survey of the WR population of the Sculptor group spiral galaxy NGC 7793.

(i) From archival narrow-band imaging, we identify 74 candidate emission-line regions, of which 39 have been spectroscopically observed with the MOS mode of FORS1. Of these, 85 per cent of these sources exhibited WR features above a 3σ level. Additional slits were used to observe H II regions, enabling an estimate of the metallicity gradient of NGC 7793 using strong line calibrations, from which $\log(O/H)+12 = 8.61\pm0.05-(0.36\pm0.10)\, r/R_{25}$ was obtained. We have estimated WR populations using a calibration of line luminosities of LMC stars, revealing ∼27 WN and ∼25 WC stars for sources spectroscopically observed.

(ii) Photometric properties of the remaining candidates suggest an additional ∼27 WN and ∼8 WC stars. In addition, a comparison with LMC WR stars degraded to the spatial resolution achieved for NGC 7793 suggests that our imaging survey has identified ∼80 per cent of WN stars and ∼90 per cent for the WC subclass, from which a total of 68 WN and 37 WC stars are inferred within NGC 7793, i.e. N(WC)/N(WN) ∼ 0.5

(iii) Our H II region spectroscopy permits an updated SFR of 0.45 $M_{\odot}$ yr^{-1} with respect to Kennicutt et al. (2008), from which N(WR)/N(O) ∼ 0.017 is obtained, assuming N(O)/N(O7V) ∼ 1.5. A comparison between the WR census of NGC 7793 and survey of the central region of NGC 300 by Schild et al. (2003) is carried out. This reveals somewhat higher N(WR)/N(O) and N(WC)/N(WN) ratios in NGC 300, in part anticipated owing to its slightly higher mean metallicity.

(iv) NGC 7793 represents the fourth of 10 star-forming spiral galaxies within 2–8 Mpc whose WR populations that we are surveying. Once completed, these will provide a data base from which the nature of a future Type Ib/c supernova can be investigated.

(v) Therefore, we have considered biases arising from differences between the intrinsic line strengths of WN and WC stars plus ground-based spatial resolution limitations. Therefore, we consider (a) the LMC WR population degraded to that if it was located at a distance of 4 Mpc; (b) differences to the apparent magnitude to the subset of NGC 7793 sources resulting from higher spatial resolution *HST*/ACS imaging. Upcoming narrow-band WFC3 *HST* imaging of the grand-design spiral galaxy M101 (PI: M. Shara) will therefore provide the ideal data set with which to assess the nature of its future ccSNe. This complements both our ground-based studies and the WFPC2 survey of the nearby late-type spiral NGC 2403 by Drissen et al. (1999).

(vi) Finally, we also report the fortuitous detection of a bright ($m_{\rm V}$ = 20.8 mag) background quasar Q2358-32 at z ∼ 2.02 resulting from C IV λ1548-51 redshifted to the λ4684 passband.

ACKNOWLEDGMENTS

JLB acknowledges financial support from STFC. Some of the data presented in this paper were obtained from the Multimission Archive at the Space Telescope Science Institute (MAST). STScI is operated by the Association of Universities for Research in Astronomy, Inc., under NASA contract NAS5-26555. Support for MAST for non-*HST* data is provided by the NASA Office of Space Science via grant NAG5-7584 and by other grants and contracts. Support for some of this work, part of the Spitzer Space Telescope Legacy Science Programme, was provided by NASA through contract 1224769 issued by the Jet Propulsion Laboratory, California Institute of Technology under NASA contract 1407.

REFERENCES

Abbott J. B., Crowther P. A., Drissen L., Dessart L., Martin P., Boivin G., 2004, MNRAS, 350, 552

Bowen D. V., 1991, MNRAS, 251, 649
Bresolin F., Schaerer D., González Delgado R. M., Stasińska G., 2005, A&A, 441, 981
Bresolin F., Gieren W., Kudritzki R., Pietrzyński G., Urbaneja M. A., Carraro G., 2009, ApJ, 700, 309
Breysacher J., Azzopardi M., Testor G., 1999, A&AS, 137, 117
Carignan C., Puche D., 1990, AJ, 100, 394
Chun M.-S., 1983, J. Korean Astron. Soc., 16, 1
Conti P. S., Vacca W. D., 1990, AJ, 100, 431
Conti P. S., Crowther P. A., Leitherer C., 2008, From Luminous Hot Stars to Starburst Galaxies. Cambridge Univ. Press, Cambridge
Corwin H. G., Jr, Buta R. J., de Vaucouleurs G., 1994, AJ, 108, 2128
Crowther P. A., 2007, ARA&A, 45, 177
Crowther P. A., Bibby J. L., 2009, A&A, 499, 455
Crowther P. A., Dessart L., 1998, MNRAS, 296, 622
Crowther P. A., Hadfield L. J., 2006, A&A, 449, 711
Crowther P. A., Smith L. J., 1997, A&A, 320, 500
Crowther P. A., De Marco O., Barlow M. J., 1998, MNRAS, 296, 367
Crowther P. A., Dessart L., Hillier D. J., Abbott J. B., Fullerton A. W., 2002, A&A, 392, 653
Crowther P. A., Drissen L., Abbott J. B., Royer P., Smartt S. J., 2003, A&A, 404, 483
Crowther P. A., Carpano S., Hadfield L. J., Pollock A. M. T., 2007, A&A, 469, L31
Crowther P. A., Barnard R., Carpano S., Clark J. S., Dhillon V. S., Pollock A. M. T., 2010, MNRAS, 403, L11
Davoust E., de Vaucouleurs G., 1980, ApJ, 242, 30
de Vaucouleurs G., de Vaucouleurs A., Corwin H. G., Jr, Buta R. J., Paturel G., Fouque P., 1991, 3rd Reference Catalogue of Bright Galaxies
Dopita M. A., Bell J. F., Chu Y., Lozinskaya T. A., 1994, ApJS, 93, 455
Draper P. W., Berry D. S., Jenness T., Economou F., 2009, in Bohlender D. A., Durand D., Dowler P., eds, ASP Conf. Ser. Vol. 411, Astronomical Data Analysis Software and Systems XVIII. Astron. Soc. Pac., San Francisco, p. 575
Dray L. M., Tout C. A., 2003, MNRAS, 341, 299
Drissen L., Roy J., Moffat A. F. J., Shara M. M., 1999, AJ, 117, 1249
Eldridge J. J., Vink J. S., 2006, A&A, 452, 295
Evans C. J., Lennon D. J., Trundle C., Heap S. R., Lindler D. J., 2004, ApJ, 607, 451
Evans C. J. et al., 2010, in de Gris R., Lepine J. R. D., eds, Proc. IAU Symp. Vol. 266, Star Clusters: Basic Galactic Building Blocks Throughout Time and Space. Cambridge Univ. Press, Cambridge, p. 35
Gibson B. K., 2000, Mem. Soc. Astron. Ital., 71, 693
Gieren W., Pietrzyński G., Soszyński I., Bresolin F., Kudritzki R., Minniti D., Storm J., 2005, ApJ, 628, 695
Gil de Paz A., Madore B. F., Pevunova O., 2003, ApJS, 147, 29
Hadfield L. J., Crowther P. A., 2007, MNRAS, 381, 418
Hadfield L. J., Crowther P. A., Schild H., Schmutz W., 2005, A&A, 439, 265
Hamuy M., Walker A. R., Suntzeff N. B., Gigoux P., Heathcote S. R., Phillips M. M., 1992, PASP, 104, 533
Hamuy M., Suntzeff N. B., Heathcote S. R., Walker A. R., Gigoux P., Phillips M. M., 1994, PASP, 106, 566
Hintzen P., Maran S. P., Michalitsianos A. G., Foltz C. B., Chaffee F. H., Jr, Kafatos M., 1990, AJ, 99, 45
Hummer D. G., Storey P. J., 1987, MNRAS, 224, 801
Karachentsev I. D. et al., 2003, A&A, 404, 93
Kelly P. L., Kirshner R. P., Pahre M., 2008, ApJ, 687, 1201
Kennicutt R. C., Jr, 1998, ARA&A, 36, 189
Kennicutt R. C., Jr, Bresolin F., Bomans D. J., Bothun G. D., Thompson I. B., 1995, AJ, 109, 594
Kennicutt R. C., Jr et al., 2003, PASP, 115, 928
Kennicutt R. C., Jr, Lee J. C., Funes José G. S. J., Sakai S., Akiyama S., 2008, ApJS, 178, 247
Lee J. C. et al., 2009, ApJ, 706, 599
Leloudas G., Sollerman J., Levan A. J., Fynbo J. P. U., Malesani D., Maund J. R., 2010, preprint (arXiv:1002.3164)
McCall M. L., 1982, PhD thesis, Univ. Texas
McCall M. L., Rybski P. M., Shields G. A., 1985, ApJS, 57, 1
Magrini L., Vílchez J. M., Mampaso A., Corradi R. L. M., Leisy P., 2007, A&A, 470, 865
Massey P., 1996, in Vreux J. M., Detal A., Fraipont-Caro D., Gosset E., Rauw G., eds, Liege Int. Astrophys. Colloq. Vol. 33, Wolf–Rayet Stars in the Framework of Stellar Evolution. Univ. Liege, Liege, p. 361
Massey P., Conti P. S., 1983, ApJ, 273, 576
Massey P., Holmes S., 2002, ApJ, 580, L35
Massey P., Hunter D. A., 1998, ApJ, 493, 180
Massey P., Johnson O., 1998, ApJ, 505, 793
Mazzarella J. M., Boroson T. A., 1993, ApJS, 85, 27
Meynet G., Maeder A., 2005, A&A, 429, 581
Moffat A. F. J., Shara M. M., 1983, ApJ, 273, 544
Mokiem M. R. et al., 2007, A&A, 473, 603
Mora M. D., Larsen S. S., Kissler-Patig M., Brodie J. P., Richtler T., 2009, A&A, 501, 949
O'Halloran B., Satyapal S., Dudik R. P., 2006, ApJ, 641, 795
Osterbrock D. E., 1989, Astrophysics of Gaseous Nebulae and Active Galactic Nuclei. University Science Books, Mill Valley, CA, p. 422
Pagel B. E. J., Edmunds M. G., 1981, ARA&A, 19, 77
Pettini M., Boksenberg A., 1985, ApJ, 294, L73
Pettini M., Pagel B. E. J., 2004, MNRAS, 348, L59
Pilyugin L. S., Vílchez J. M., Contini T., 2004, A&A, 425, 849
Prescott M. K. M. et al., 2007, ApJ, 668, 182
Read A. M., Pietsch W., 1999, A&A, 341, 8
Schaerer D., Vacca W. D., 1998, ApJ, 497, 618
Schild H., Smith L. J., Willis A. J., 1990, A&A, 237, 169
Schild H., Crowther P. A., Abbott J. B., Schmutz W., 2003, A&A, 397, 859
Schlegel D. J., Finkbeiner D. P., Davis M., 1998, ApJ, 500, 525
Seaton M. J., 1979, MNRAS, 187, 73
Smith L. F., Shara M. M., Moffat A. F. J., 1990, ApJ, 358, 229
Smith L. F., Shara M. M., Moffat A. F. J., 1996, MNRAS, 281, 163
Stetson P. B., 2000, PASP, 112, 925
Tody D., 1986, in Crawford D. L. ed., Proc. SPIE Vol. 627, Instrumentation in Astronomy VI. SPIE, Bellingham, p. 733
Torres-Dodgen A. V., Massey P., 1988, AJ, 96, 1076
Urbaneja M. A. et al., 2005, ApJ, 622, 862
Walborn N. R., Drissen L., Parker J. W., Saha A., MacKenty J. W., White R. L., 1999, AJ, 118, 1684
Webster B. L., Smith M. G., 1983, MNRAS, 204, 743
Woosley S. E., Bloom J. S., 2006, ARA&A, 44, 507

SUPPORTING INFORMATION

Additional Supporting Information may be found in the online version of this article:

Figure 2. Finding charts.
Table 3. Catalogue of nebular fluxes within H II regions in NGC 7793.

Please note: Wiley–Blackwell are not responsible for the content or functionality of any supporting materials supplied by the authors. Any queries (other than missing material) should be directed to the corresponding author for the article.

This paper has been typeset from a TEX/LATEX file prepared by the author.